SKB

TECHNICAL REPORT 97-21

Investigation of the large scale regional hydrogeological situation at Ceberg

Anders Boghammar[1], Bertil Grundfelt[1], Lee Hartley[2]

1 Kemakta Konsult AB, Sweden
2 AEA Technology, UK

November 1997

SVENSK KÄRNBRÄNSLEHANTERING AB
SWEDISH NUCLEAR FUEL AND WASTE MANAGEMENT CO

P.O.BOX 5864 S-102 40 STOCKHOLM SWEDEN
PHONE +46 8 459 84 00
FAX +46 8 661 57 19

INVESTIGATION OF THE LARGE SCALE REGIONAL HYDROGEOLOGICAL SITUATION AT CEBERG

Anders Boghammar1, Bertil Grundfelt[1], Lee Hartley[2]

1 **Kemakta Konsult AB, Sweden**
2 **AEA Technology, UK**

November 1997

This report concerns a study which was conducted for SKB. The conclusions and viewpoints presented in the report are those of the author(s) and do not necessarily coincide with those of the client.

Information on SKB technical reports from1977-1978 (TR 121), 1979 (TR 79-28), 1980 (TR 80-26), 1981 (TR 81-17), 1982 (TR 82-28), 1983 (TR 83-77), 1984 (TR 85-01), 1985 (TR 85-20), 1986 (TR 86-31), 1987 (TR 87-33), 1988 (TR 88-32), 1989 (TR 89-40), 1990 (TR 90-46), 1991 (TR 91-64), 1992 (TR 92-46), 1993 (TR 93-34), 1994 (TR 94-33), 1995 (TR 95-37) and 1996 (TR 96-25) is available through SKB.

INVESTIGATION OF THE LARGE SCALE REGIONAL HYDROGEOLOGICAL SITUATION AT CEBERG

Anders Boghammar[1]
Bertil Grundfelt[1]
Lee Hartley[2]

[1]Kemakta Konsult AB
[2]AEA Technology UK

6th November 1997

Abstract

The present study forms part of the large-scale groundwater flow studies within the SR 97 project. The site of interest is Ceberg.

Within the present study two different regional scale groundwater models have been constructed, one large regional model with an areal extent of about $300km^2$ and one semi-regional model with an areal extent of about $50km^2$.

Different types of boundary conditions have been applied to the models. Topography driven pressures, constant infiltration rates, non-linear infiltration combined specified pressure boundary conditions, and transfer of groundwater pressures from the larger model to the semi-regional model.

The present study has shown that:

- Groundwater flow paths are mainly local. Large-scale groundwater flow paths are only seen below depth of the hypothetical repository (below 500 metres) and are very slow.
- Locations of recharge and discharge, to and from the site area are in the close vicinity of the site.
- The low contrast between major structures and the rock mass means that the factor having the major effect on the flowpaths is the topography.
- A sufficiently large model, to incorporate the recharge and discharge areas to the local site, is in the order of kilometres.
- A uniform infiltration rate boundary condition does not give a good representation of the groundwater movements in the model.
- A local site model may be located to cover the site area and a few kilometres of the surrounding region. In order to incorporate all recharge and discharge areas within the site model, the model will be somewhat larger than site scale models at other sites. This is caused by the fact that the discharge areas are divided into three distinct areas to the east, south and west of the site.
- Boundary conditions may be supplied to the site model by means of transferring groundwater pressures obtained with the semi-regional model.

Abstract (Swedish)

Den aktuella studien är en del av den storskaliga grundvattenmodellering som utförs inom SR 97. Den aktuella platsen för denna studie är Ceberg.

Två olika regionala grundvattenflödesmodeller har konstruerats, en stor modell med en ungefärlig utsträckning av 300 km^2 och en mindre modell med en ungefärlig utsträckning av 50 km^2.

Olika typer av randvillkor har testats på båda modellerna. De randvillkor som studerats är för överytan topografistyrt tryck, konstant infiltration samt ett icke-linjärt randvillkor i vilket infiltrationshastigheten är beroende av grundvattenytans läge. Dessa randvillkor har i den mindre modellen kombinerats med ansatt hydrostatiskt tryck och tryck som överförts från den större till den mindre modellen.

Den aktuella studien visar att:

- Grundvattenflödet är till största delen lokalt styrt. Storskaliga grundvattenrörelser syns endast på djup under nivån för det hypotetiska förvaret (under 500 meter) och dessa rörelser är mycket långsamma.

- In- och utströmningsområdena för det vatten som passerar genom förvarsområdet ligger i förvarets närhet.

- Den låga konduktivitetskontrasten mellan sprickzoner och bergmassa medför att flödet i området är styrt huvudsakligen av topografin.

- En modell som inkluderar alla väsentliga in- och utströmningsområden har några kilometers utbredning.

- En konstant och uniform infiltration som randvillkor ger inte en riktig bild av grundvattenrörelserna.

- En lokal modell kan inplaceras inom ett par kilometer runt förvarsområdet. För att få med alla in- och utströmningsområden i den lokala modellen behöver denna vara något större än tidigare framtagna lokalmodeller. Detta beror på att utströmningsområdena är uppdelade i tre olika delområden belägna öster, söder och väster om förvarsområdet.

- Randvillkor kan överföras till en lokal modell genom att överföra grundvattentryck som beräknats i den mindre regionala modellen.

Contents

List of Tables

List of Figures

1 Background and Objectives

The Swedish Nuclear Fuel and Waste Management Company (SKB) has initiated a safety assessment project called SR 97, which is related to safety assessment of hypothetical disposal sites for spent nuclear fuel. SR 97 is part of several performance assessments and will focus on the long term safety of disposed nuclear fuel. Three sites will be studied, Aberg, Beberg and Ceberg, data for these three sites have been taken from three real sites where SKB has performed extensive investigations. The three sites are Äspö, Finnsjön and Gideå respectively.

The present report concerns the large-scale regional groundwater flow at the Ceberg site.

The main objectives of this project are to:

1. Understand the large-scale groundwater flow patterns within the area under natural conditions.
2. Identify locations of significant recharge and discharge.
3. Examine the influence of different types of boundary conditions on the groundwater flow patterns.
4. Determine the spatial extent of the regional model required to predict groundwater flow patterns in the vicinity of the site.
5. The results of this work will be used to select the location of a site scale model, and also supply such a model with appropriate boundary conditions.

A short introduction and a brief description of the various modelling cases performed is described in Chapter 2. The geohydrology data as used in this project is described in Chapter 3. Chapter 4 presents the results from a large regional model along with a description of the numerical model. The smaller regional model is discussed in Chapter 5. Discussion and conclusions are found in Chapters 6.

2 Introduction

The following Sections describe the concepts, methods and assumptions used.

2.1 Site Location

The modelling performed concerned the Ceberg site within SR 97. The Ceberg site is based on data from the Gideå site which is located 10 km from the coast and at an elevation of approximately 100 metres above sea level. Figure 2.1 shows the location of the Ceberg site.

The site area is rather flat and surrounded by a couple of lakes, rivers and marshes. There is a ridge coming from the northwest just above the site.

The coordinate system used is the National Swedish RAK-system, with offset in East-West of 1 650 000 m and in North-South of 7 030 000 m. All plots in this report refers to this coordinate system.

2.2 Modelling Techniques

The modelling of the groundwater flow has been carried out with the finite element code NAMMU [*Cliffe et al., 1995*] using deterministic properties. NAMMU uses a porous medium approach.

Fracture zones have been modelled using an implicit method whereby the fractures are modelled by modifying the hydraulic conductivities of the rock mass at the location of the fracture zones [*Boghammar et al., 1992*], a description of this method is included as Appendix A.

2.3 Boundary Conditions

One of the objectives of this study is to assess how sensitive model predictions are to different types of boundary conditions. It is also important to consider what physical constraints are imposed on the system by setting a particular boundary condition, and what can be understood from the results. The four types of boundary condition were considered:

1) specified head distribution on the top surface and no flow on the lateral sides

2) specified infiltration on the lateral top surface and hydrostatic pressure on the lateral boundaries;

3) a non-linear condition on the top surface which allows both recharge and leakage and no flow on the lateral sides.

4) interpolation from larger scale model

The bottom boundary is always set to no flow

2.3.1 Regional Topographic Heads

For this case, heads on the top surface are imposed from topography and a no-flow boundary condition is applied on the lateral boundaries. This is reasonable as the vertical boundaries lie along flow divides, such as hills, valleys and lakes. On the top 50 m of the lateral boundaries a boundary condition equivalent to a hydrostatic pressure (a uniform pressure in the vertical direction such that the total pressure equals zero at the surface). It has been judged that 50 meters is a reasonable level to have this pressure boundary condition since it corresponds to the thickness of the permeable near-surface layers.

Remarks:

i) Gives a realistic distribution of groundwater head near surface, albeit local gradients may be overestimated near steep slopes.

ii) Regions of recharge and discharge can be identified from the vertical component of velocity.

iii) Since both recharge and discharge are possible at the top surface, pathlines can exit the domain at areas of terrestrial discharge (i.e. on the top surface).

iv) In maintaining heads at topography, very large (and probably unphysical) recharge rates can be induced especially around fracture zones and steep gradients. This can lead to high vertical velocities which can delimit local flow cells.

v) It is not possible to calibrate this type of model unless flow rate data is available. It is over-determined.

2.3.2 Uniform Infiltration

A constant infiltration rate is applied at the top surface of the model. Along the lateral sides, hydrostatic pressure is applied down to 50 metres below surface. Further down a no-flow boundary condition is applied.

Remarks:

i) Applying hydrostatic pressure down to 50 metres below surface is justified since there are not any high transmissivity zones to transmit pressures at the lateral boundaries to depth.

ii) The model can be used to calibrate permeability values for the top layers against an infiltration rate. Values are adjusted until the head field matches data or topography.

iii) Discharge can only take place at the lateral boundaries in this case. The lack of terrestrial discharge leads to the permeability being over- predicted in order to keep the heads from becoming higher than in reality.

iv) This type of boundary condition assignment allows us to see potential recharge and discharge areas by plotting total pressure.

2.3.3 Non-linear Recharge/Discharge

This is an approach to impose a distribution of recharge and discharge which is limited by a maximum potential infiltration, and allows surface runoff where the groundwater head is above the top surface. The idea is borrowed from leaky aquifer modelling. The leakage rate is a linear function of total pressure, or equivalently $(h - z)$. So where the head, h, is greater than the elevation, z, there is leakage to the environment, and where the head is less than the elevation there is infiltration up to a maximum of some specified value on infiltration, I. The boundary condition can be expressed as:

$$discharge = \begin{cases} \omega(h-z) & h > z - L \\ -I & h <= z - L \end{cases}$$

L is arbitrary, but we have chosen L equal to 5 m, i.e. we obtain maximum recharge if the head is more than 5 m below topography. This implies $\omega = I/L$ and $I \approx 2{\cdot}10^{-9}\mathrm{ms}^{-1}$ (60mm/year) which gives $\omega = 4 \cdot 10^{-10}\mathrm{s}^{-1}$. This can be considered as leakage through a 5 m layer of hydraulic conductivity $2 \cdot 10^{-9}\mathrm{ms}^{-1}$.

This is only a model. In reality, recharge is related to unsaturated conditions, and the permeability and thickness of river sediments and superficial deposits will determine discharge. Hence, using a constant ω is only an approximation. However, this method does predict a realistic behaviour.

Along the lateral sides, hydrostatic pressure is applied down to 50 metres below surface. Further down a no-flow boundary condition is applied.

Remarks:

i) A head distribution closer to topography, and reality, can be obtained using this prescription of recharge. The head distribution tends not to have as steep gradients as topography.

ii) Plots of total pressure, $P_t = P_d + P_h = \rho g(h - z)$, where P_t is total pressure, $P_h = -\rho g z$ is the hydrostatic pressure and $P_d = \rho g h$ is dynamic pressure, show regions and magnitudes of recharge and discharge.

iii) The model can be used to calibrate permeability.

iv) This recharge definition essentially acts to limit over-predictions of head by allowing for discharge.

v) Pathlines can exit on the top surface using this model.

vi) This variant can be used to examine how influential topography is in the case where a topography dependent head is applied as a boundary condition, since it predicts a smoother water table.

Table 2.1: Summary of simulated cases

Case	Description	GRL	GRS
	Boundary condition variations		
1	Top surface: Topographic head Lateral sides: No flow	GRLT	GRST
2	Top surface: Constant infiltration Lateral sides: Hydrostatic down to -50m No-flow rest	GRLI	-
3	Top surface: Non-linear infiltration Lateral sides: Hydrostatic down to -50m No-flow rest	GRLN	GRSN
4	Top surface: Transfer of pressure from larger model Lateral sides: Transfer of pressure from larger model	-	GRSL
	Conductivity variations		
5	High contrast case: fracture zone conductivity has been increased with a factor of 100.	-	GRSFH
6	No contrast case: fracture zones have been removed.	-	GRSFL
7	Uniform permeability with depth	-	GRSU
8	Hydraulic anisotropy	-	GRSA

2.4 Numerical Models

In order to be able to investigate the effect of different boundary conditions on simulating large-scale groundwater flow patterns, two different models have been created, one large regional model, GRL, with an areal extent of approximately 300 km^2, and a smaller regional model, GRS, with an areal extent of approximately 50 km^2. Both models extend to a depth of -1500 meters. For a short description of the keyvalues for the two model refer to Tables 4.1 and 5.1.

The large regional model was made large enough to incorporate all potential recharge and discharge areas whereas the smaller regional model has an extent dictated by the structural and topographical information given. Hence, the domain of the smaller model was not created based on any information from the larger model. Figure 2.1 shows the location of the boundaries of the two models. The models are outlined in green.

The boundaries of both models have mainly been located along fracture zones. It may be debated whether it is correct to assign a no-flow boundary condition on these boundaries as outlined in Section 2.3, considering the fact that the contrast in hydraulic conductivity between the rock mass and the fracture zones is low. The choice of using no-flow can be justified by the fact that the bounding fracture zones are located along rivers and valleys and will therefore most likely act as some sort of water divides. This is of course not necessarily true, but it is a fair generalization and other types of boundary conditions that may be applied along these boundaries, would probably not significantly alter the situation in the area of interest for this study.

In addition to the different boundary conditions a set of conductivity variations have been studied for the small regional model to show the effect of the heterogeneity in the hydraulic conductivity on the general flow pattern. Table 2.1 shows a summary of the various cases.

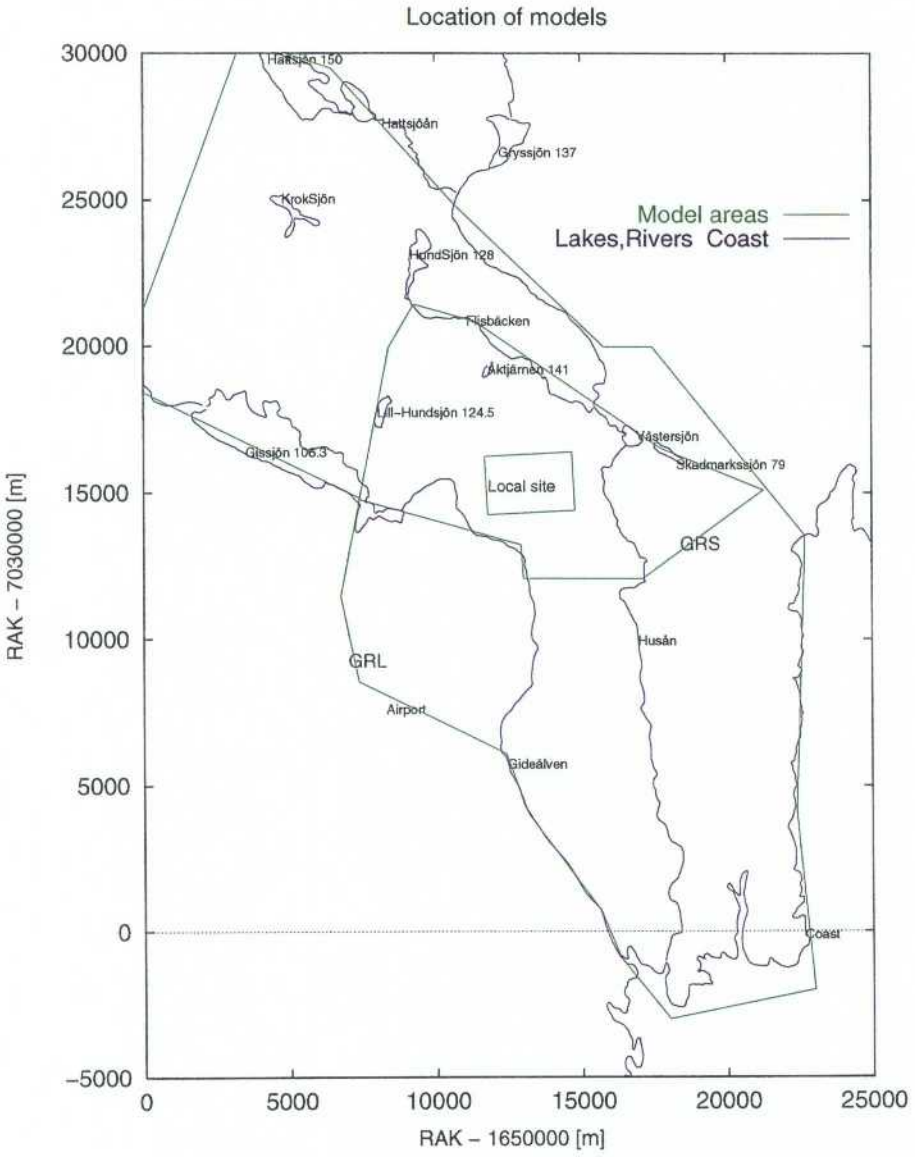

Figure 2.1: Location of the large and small regional models at Ceberg which corresponds to the Gideå test site. The two models have been outlined in green. The location of the site area is indicated by a box labeled Site. Note the horizontal axis corresponds to W-E, and the vertical axis to S-N.

3 Geohydrology at the Ceberg site

3.1 Topography

Topography data was obtained using the SKB GIS database. The topography on the large scale is shown in Figure 3.1. Topography data has been used to adjust the top surface of the finite- element meshes.

3.2 Structural Model

Douglas Walker [*Walker et al., 1997*] has compiled the geohydrology data and information for all three sites in SR 97. Much of the methodology has been taken from [*Rhén et al., 1997*]. Specifically for Ceberg the analysis is based on the structural geology model as worked out by [*Hermansson et al, 1997*]. Hermansson focused on site scale but also includes some discussion on the larger scale. The work by Walker resulted in two sets of regional fracture zones, one set was marked as well expressed and the other set was marked as less well expressed.

The total number of fracture zones used in the regional scale model (GRL) was 51. In the present work only the well expressed zones have been included along with the site scale fracture zones and some of the less well expressed. The reason for including some of the less well expressed zones was to get a hydraulic connection between the site scale zones and the regional zones since none of the well expressed zones intersected the site area. The less well expressed zones included are the ones that have been identified as part of the site scale structural model. To include all less well expressed zones was not feasible.

The model used consists of 39 regional zones and 12 site scale zones and is shown in Figure 3.2.

All regional zones in the model have a width of 20 m and are all dipping 90°. This is also true for the site scale zones, although some of these have been specified with a dip. It was concluded that this assumption would hold in the regional models with a coarse grid resolution of 500 m in the horizontal directions.

In addition, the site scale zones have only been modelled as straight lines between the horizontal end points.

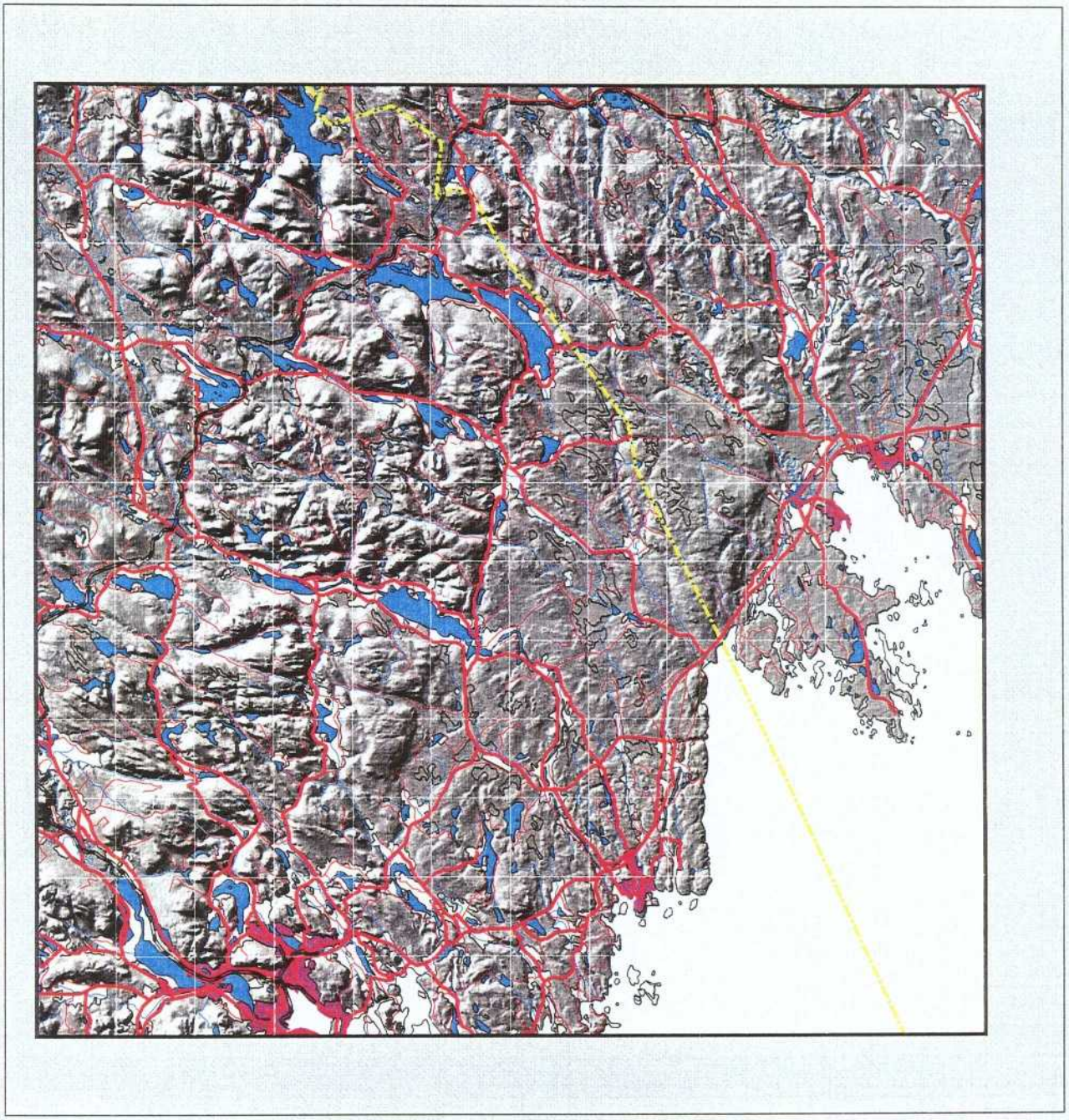

Figure 3.1: Topography on a large scale. Map has been supplied by the SKB GIS system.

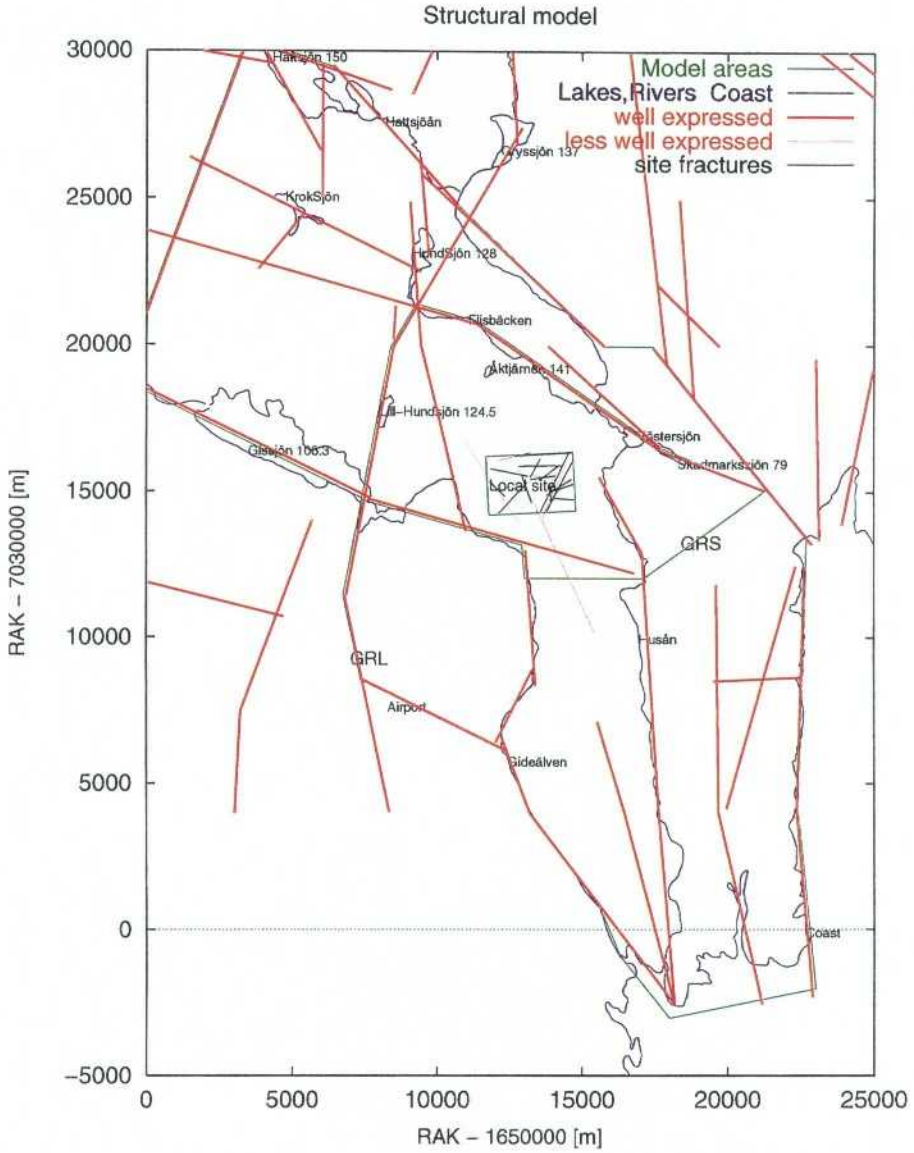

Figure 3.2: Structural model used including all the well expressed zones, the site scale zones and some of the less well expressed zones.

3.3 Hydrogeological Properties

[*Walker et al., 1997*] collated structural data for regional fracture zones. Hydrogeological properties were also sourced from Doug Walker. The conclusions of the data analysis carried out by Walker can be summarised:

i) hydraulic conductivity decreased with depth in a stepwise fashion;

ii) central values for the regional rock domain (RRD1) at the 100m scale ranged between $10^{-7.2}$m/s at surface and $10^{-9.8}$ m/s below a depth of 300m;

iii) central values for the regional conducting domain (RCD1), that is the fracture zones, at the 100m scale ranged between $10^{-6.4}$ at surface and $10^{-9.1}$ m/s below a depth of 300m;

iv) the hydraulic conductivity of the fracture zones was about 6 times that of the rock mass.

Walker et al. [*1997*] suggests a variance of less than 1 in the logarithm of hydraulic conductivity for the rock mass, but puts a greater uncertainty on the hydraulic conductivity of the fracture zones. The main question being whether the regional lineaments are flowing features, since it is possible some may have been mineralised to create flow barriers. Hence, it was considered necessary to quantify the sensitivity to the hydraulic conductivity of the fracture zones by a series of scoping studies.

Figure 3.3 shows the hydraulic conductivities used, as a function of depth. The values are consistent with the ones supplied by Walker et al. [*1997*], they only differ in the topmost part of the model where a calibration had to be performed in order to get a consistent water balance and head distribution. Merely using the given values on conductivity and the topography as top surface boundary condition, gave unrealistic infiltration rates in the orders of metres per second. The near surface head distribution is expected to be a subdued, smoothed version of topography, as verified by the study of Timje [*1983*] to assess the regional groundwater table. Further seasonal fluctuations have been shown to be at most 4m [*Ahlbom et al., 1983*], which suggests the unsaturated zone is only a few metres in thickness. Hence, in calibrating the infiltration and hydraulic conductivity it was assumed that the actual near surface head distribution is close to topography. More detail on the calibration is given in Subsection 4.3.2.

The conductivities were assigned by first setting a uniform conductivity for all elements and then multiplying that value with a factor to obtain the desired stepwise depth dependency function. The base values used are for the fracture zones, RCD1, $8.71 \cdot 10^{-10}(10^{-9.1})$ and for the rock mass, RRD1, $1.48 \cdot 10^{-10}(10^{-9.8})$.

For part of the model north of the ridge near zone GR02, the conductivity has further been multiplied by a factor of 0.1 in order to get the calculated heads consistent with the topography data.

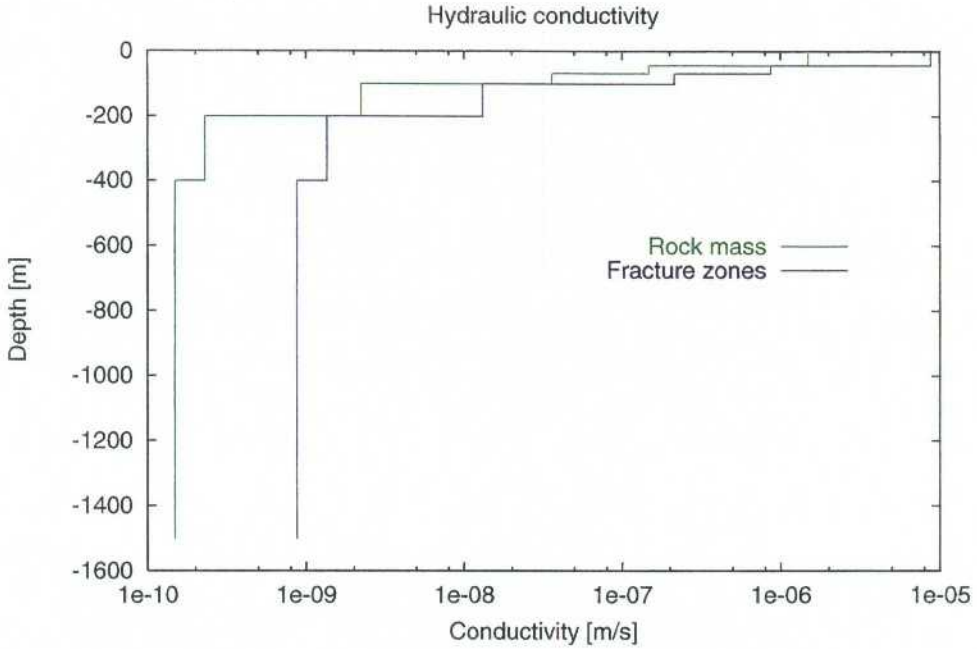

Figure 3.3: Hydraulic conductivities for the rock mass (green) and fracture zones (blue) used in the modelling . The conductivities follow the stepwise function with depth as given by Walker et al. [*1997*], apart for the topmost three layers of elements (approximately down to 50 meters depth), where a calibration had to be performed.

Table 3.1: Depth dependency of the hydraulic conductivity used for individual elemental layers within the models along with the depth of the element centroid. The first three element layers deviate from the values given by [*Walker et al., 1997*] since these were modified during the calibration.

Element layer	**Conductivity used for zones, RCD1**	**Conductivity used for rock, RRD1**	**Depth of element centroid**
	$[m/s]$	$[m/s]$	$[m]$
1	$8.71 \cdot 10^{-6}$	$1.48 \cdot 10^{-6}$	-5.0
2	$8.71 \cdot 10^{-6}$	$1.48 \cdot 10^{-6}$	-17.5
3	$8.71 \cdot 10^{-6}$	$1.48 \cdot 10^{-6}$	-34.0
4	$8.63 \cdot 10^{-7}$	$1.47 \cdot 10^{-7}$	-55.5
5	$2.13 \cdot 10^{-7}$	$3.61 \cdot 10^{-8}$	-83.9
6	$1.31 \cdot 10^{-8}$	$2.22 \cdot 10^{-9}$	-150.0
7	$1.35 \cdot 10^{-9}$	$2.29 \cdot 10^{-10}$	-250.0
8	$1.35 \cdot 10^{-9}$	$2.29 \cdot 10^{-10}$	-350.0
9	$8.71 \cdot 10^{-10}$	$1.48 \cdot 10^{-10}$	-450.0
19	$8.71 \cdot 10^{-10}$	$1.48 \cdot 10^{-10}$	-550.0
11	$8.71 \cdot 10^{-10}$	$1.48 \cdot 10^{-10}$	-750.0
12	$8.71 \cdot 10^{-10}$	$1.48 \cdot 10^{-10}$	-1050.0

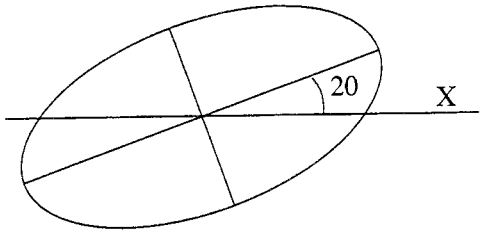

Figure 3.4: Schematic diagram showing the principal and minor axes of hydraulic conductivity in the horizontal plane for the anisotropic case. The principal direction of the anisotropy has been rotated 20°counterclockwise (N20W) compared to the Cartesian co-ordinate system used within the model. Note that the scaling of the principal and minor axes is not proportional, it should be 100:1.

An anisotropic case has also been studied. The anisotropy is described with the major axis scaled according to the ratios 1:0.01:0.01 in X, Y and Z respectively and the system rotated in the horizontal plane 20° counter clockwise. These values have been estimated taking the major rock stress into account [*Walker et. al., 1997*]. Figure 3.4 shows a representation of the anisotropy in the horizontal plane.

When modelling the anisotropy, only those elements that were assigned as rock mass have been made anisotropic. This is due to the way the implicit fracture zone method works, see Appendix A.

4 Large Regional Model - GRL

4.1 Location and Size

The boundaries of the Large Regional Model (GRL) were chosen to be sufficiently distant so that all possible recharge and discharge areas, which might influence flow at the site, were within the simulation domain, see Figure 2.1.

The model extends for about 30km from Hattsjön in the North to the coast at Husum in the South, and from Gissjön in the West eastwards to the coast, a distance of about 24km. The boundaries of the model are associated with river valleys, the coastline, or regional fracture zones. Several lakes, rivers and streams are included in the model. Gissjön and Gideälven form part of the SouthWest boundary, Hattsjöån and Husån form part of the northern boundary. Gideälven, Husån and Flisbacken flow through the modelled region. Each of these lakes and water courses provide potential areas for groundwater discharge, suggesting there may be substantial terrestial discharge within this model.

The anticipated general synopsis is that recharge will take place on the high ground in the North West, which will drive flow toward the coast in the East and South East, along with some discharge to rivers and lakes.

4.2 Finite-Element Mesh

The finite element grid constructed for the GRL model has the key values shown in Table 4.1. Figure4.1 shows a top view of the mesh. The local site area is outlined as a square in the middle of the model. The top surface of the model was adjusted to fit the topography of the area. Topography data was obtained using the SKB GIS database.

Table 4.1: Key values for the GRL finite element grid.

Item	Value
Number of elements	23725
Number of nodes	26936
Depth	-1500 masl
Areal extent	30x10 km
Front width	392
Approximate horizontal resolution	500 m

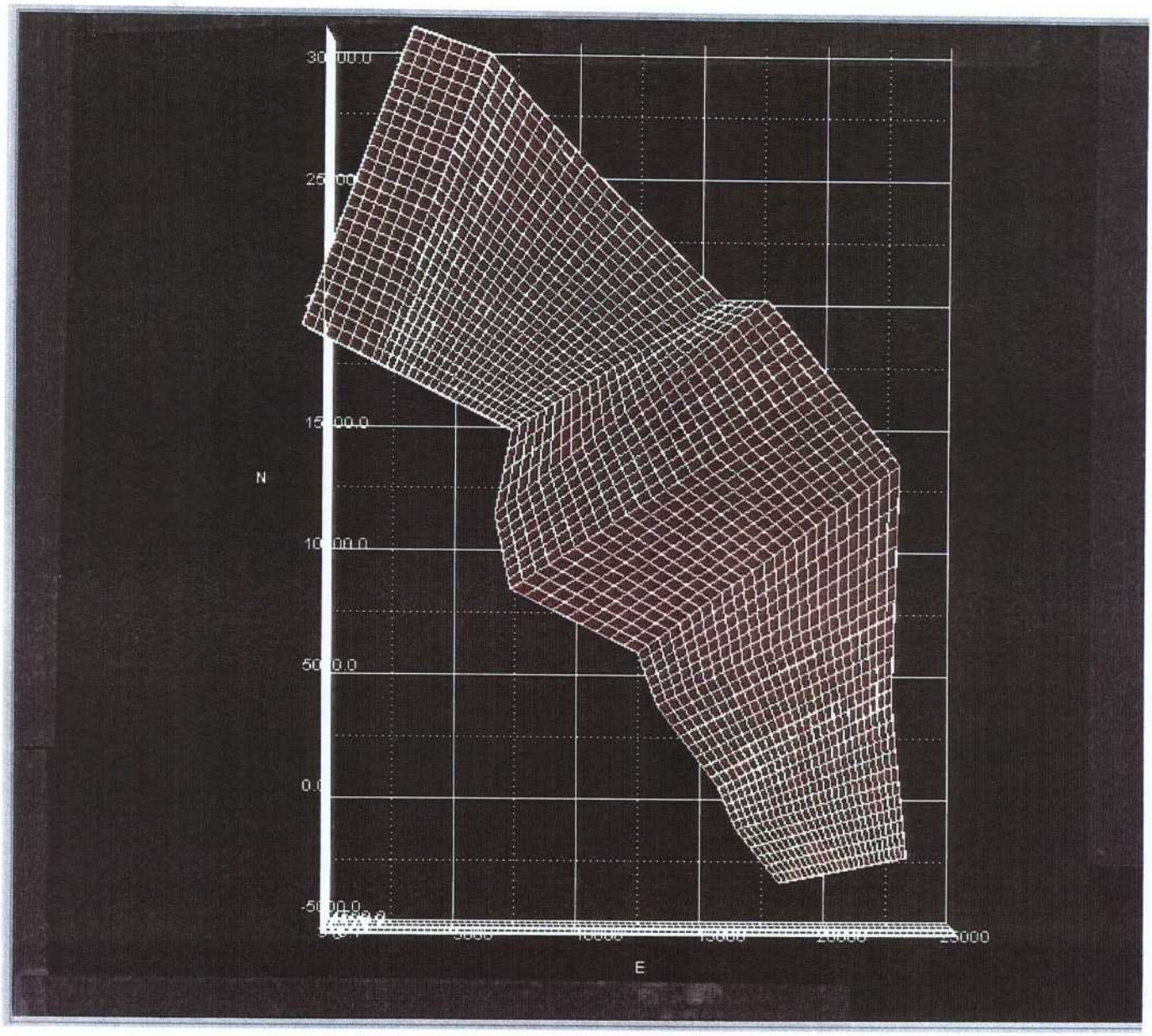

Figure 4.1: Top view of the finite element mesh for the large regional model, GRL.

4.3 Boundary Condition Variations

One of the objectives of this study is to assess how sensitive model predictions are to different types of boundary conditions. The prescription and results of each of these cases is described in the following subsections.

4.3.1 Specified Pressure (GRLT)

This formed the base case for the GRL. The pressure on the top surface was fixed such that the groundwater head equated to the height of topography. A no-flow boundary was imposed on the lateral boundaries apart from the top 50m of boundary that runs along the coastline where a hydrostatic boundary was specified.

Since the permeability of the rock mass is so low, it is realistic to assume that the water table is close to ground surface. However, local pressure gradients may be over- predicted near fracture zones and steep slopes in the topography. In such circumstances, the recharge rates required to maintain heads at topography can exceed the potential infiltration available, and hence are unphysical. The mean precipitation in the Gideå area is about 765mm/year of which about 33% falls as snow [*Carlsson et al.*]. The advantages of this type of boundary conditions are that the locations and quantities of both recharge and discharge are calculated automatically. They are determined by the specified permeability field and the pressure distribution on the top surface. It is also a boundary condition that is very easy to implement. The disadvantage is that it is impossible to calibrate the model unless flow rate data is available. That is, unless there is good data on the permeability field, then it is hard to quantify how reliably the model is predicting the flow field. The choice of no-flow boundary conditions on the lateral boundaries to the North, West and South West is justified since these are either river valleys or regional fracture zones, and so are likely to be associated with water divides.

The model which will be referred to as GRLT, had a hydraulic permeability of $10^{-13}m^2$ specified in the top 3 layers of finite-elements (about 43m in thickness). The remaining 10 layers were assigned values using the depth-dependence defined by [*Walker et al., 1997*] The permeability profile is shown in Figure 3.3 (plot of function K=K(z) and values used in each layer also showing the thickness of each layer) and in Table 3.1.

The complex topography of the region is clearly shown by the distribution of pressure on the top surface, see Figure 4.2. The site itself has a low ridge running through its centre from NNW to SSW, with valleys to the East and West.

Figure 4.3 shows the distribution of flow near the surface. Again, it is seen there are very pronounced local variations. The same is true at depth. This suggests that there is a strong correlation between topography variations and the flow field in the underlying rock, and hence it may be concluded that the flow field at the site will be strongly controlled by local topography. This is confirmed by the forward and backward pathlines presented in Figure 4.4.

For the forward pathlines, 16 particles were started within the site boundary at z =

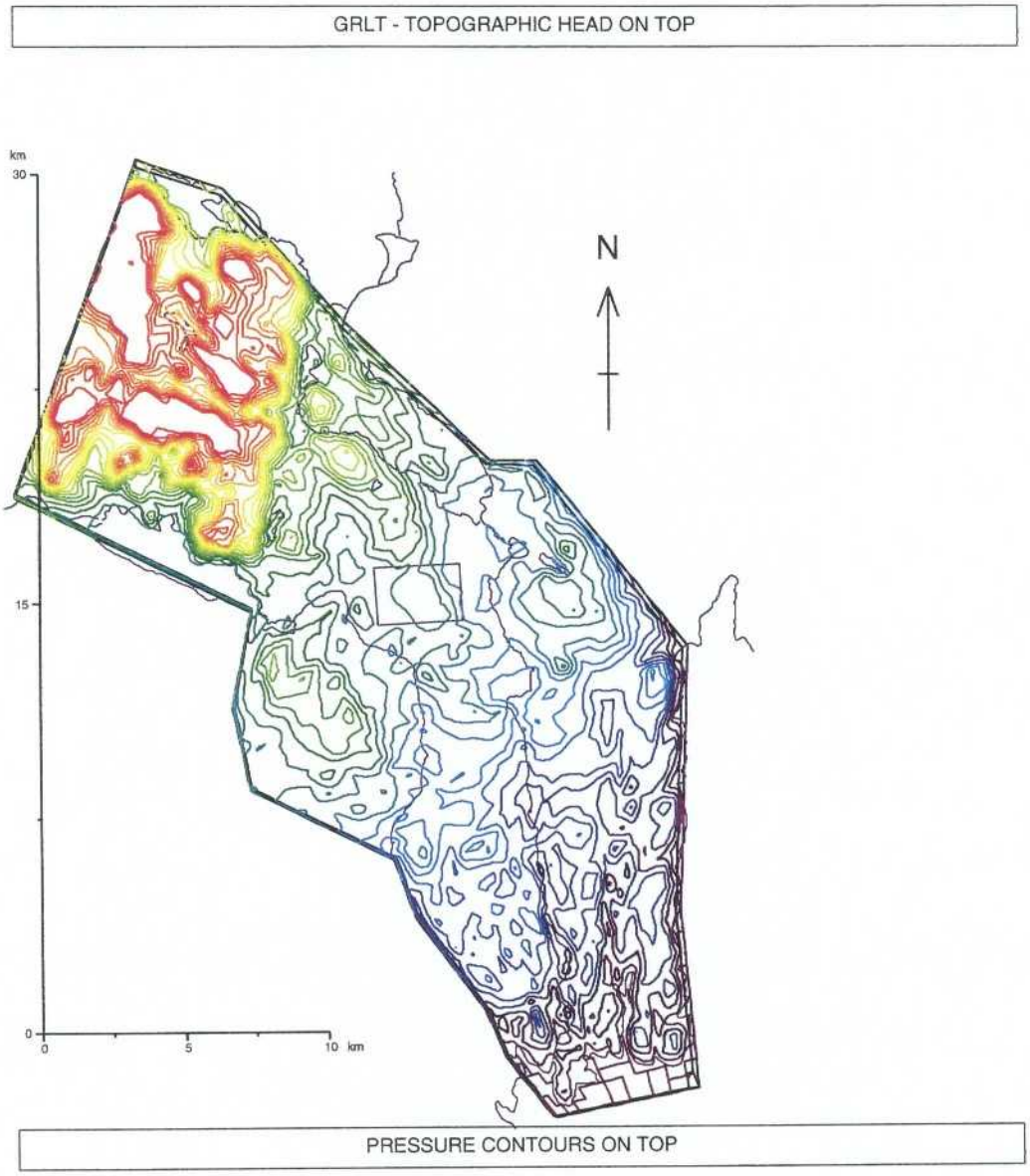

Figure 4.2: Pressure at top surface of base case large regional model (GRLT). High pressures in red and low in blue.

Figure 4.3: Flow distribution near the surface (GRLT).Arrows are coloured according to the logarithmic absolute value on the flow rate. Colors range from orange(0.0) over green(-10.0) to purple(-25.0). Arrows are three dimensional and projected onto a 2D plane, hence the arrows only show the direction of flow and the size is only an effect of the projection.

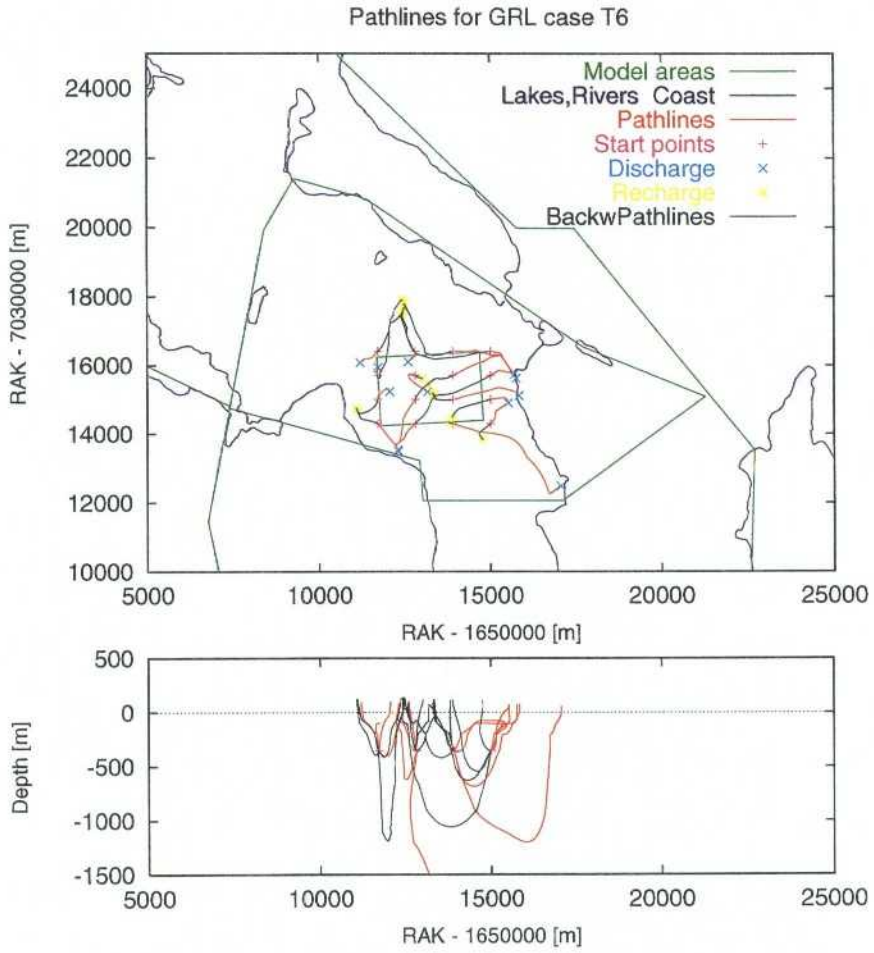

Figure 4.4: Forward(red) and backward(black) pathlines for case GRLT.

-350m and tracked with the flow until they exited the domain on the top surface. Particles starting in the East discharged at Husån about 1km to the East. For start positions in the NW they discharge on slopes facing Torstorsselet slightly to the West, and in the South East, particles discharge near Gideåbruk in the South. For backward pathlines, particles are started at the same locations, but tracked upstream against the flow to areas of recharge on the top surface. It is seen that most of the groundwater recharge to the site comes from the ridge around Ormyran in the centre of the site. Bodinsberget, about 1km to the NW, feeds recharge in the Northern part of the site. Torrberget slightly to the West also provides a small recharge to the SW of the site.

Pressure contours and flow vectors on vertical slices can also be used to understand the flow field. Figures 4.5 and 4.6 show the dynamic pressure distribution and flow vectors, respectively, for a slice running from the NW corner (approximately at -1000, 19000) to the SE corner (23000,14000) of the model and passing through the site.

The general trend is that the dynamic pressure decreases from NW to SE, as expected. However, there are a number of U-shaped contours extending down from the surface. These are associated with significant vertical flows, as can be seen in the flow vector plots of Figure 4.6. It is further confirmation that the undulating topography around the site gives rise to a considerably variable flow pattern and distribution of recharge/discharge. Indeed the flow pattern is governed by local flow cells.

Figure 4.7 shows the distribution of recharge and discharge on a regular mesh of points within a horizontal slice near the top surface. Flow vectors indicate the direction of the flow in three-dimensions, but are coloured according to the direction (up/down) and magnitude of the vertical flow. Recharge is coloured in colours from red to green, red corresponding to the highest magnitude. Discharge is coloured from violet to cyan, violet corresponding to the highest discharge.

There is no consistent trend in the distribution in recharge and discharge across the whole domain, but the localised regions of discharge seem coincident with streams and lakes, and the recharge occurs where topography is relatively high, as expected. Mean rates of infiltration are in the order of $10^{-9} ms^{-1}$, which is about 50mm/year. This value is consistent with the values reported by Walker et al [*1997*]. From this, one may conclude that the values of permeability chosen are about the right order of magnitude to give a water balance which is physically realistic for a fractured granitic rock. The maximum infiltration is about $3 \cdot 10^{-8} ms^{-1}$, or about 1m/year. It suggests that in some places the amount of recharge necessary to maintain the water table at the ground surface cannot be achieved physically, and so the water table in reality is at least several metres below ground surface.

4.3.2 Specified Infiltration Boundary Condition (GRLI)

This case was calibrated by assigning a 50mm/year infiltration on the top surface and adjusted the conductivities in the top layers to get a good fit to general pressure distribution, assuming that the general pressure distribution equals the topography. The same hydraulic conductivity, $10^{-6} ms^{-1}$, was applied to the top layers to get a

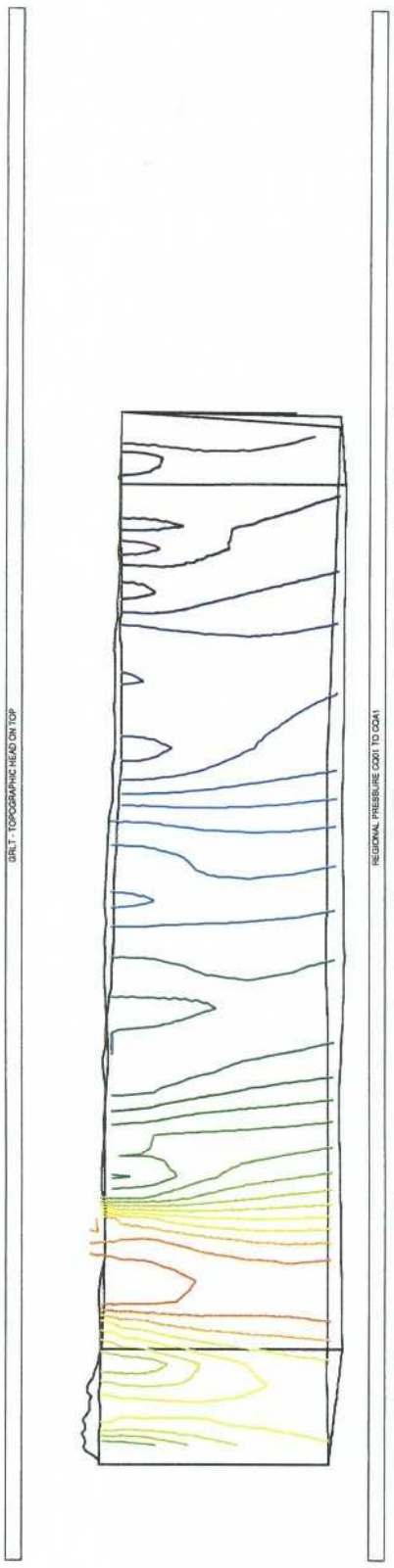

Figure 4.5: Vertical slice with contours of dynamic pressure (GRLT). The slice runs through the site area in an ESE-WNW direction.

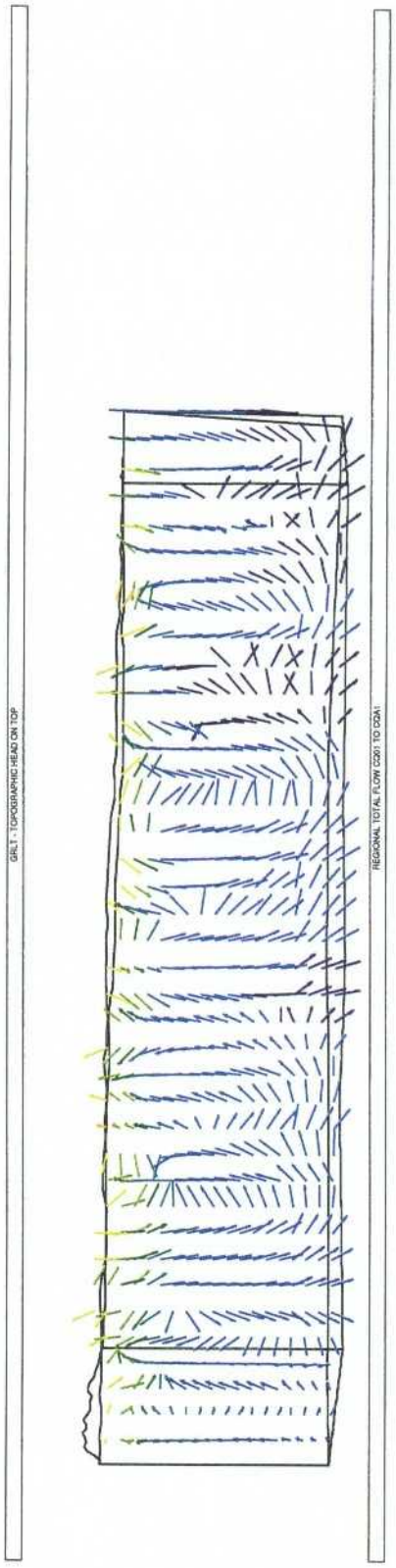

Figure 4.6: Vertical slice with flow vectors (GRLT). The slice goes through the site area in an ESE-WNW direction. The flow vectors are 3D vectors projected on a 2D plane the size of the flow is indicated by the colour scheme according to figure 4.3.

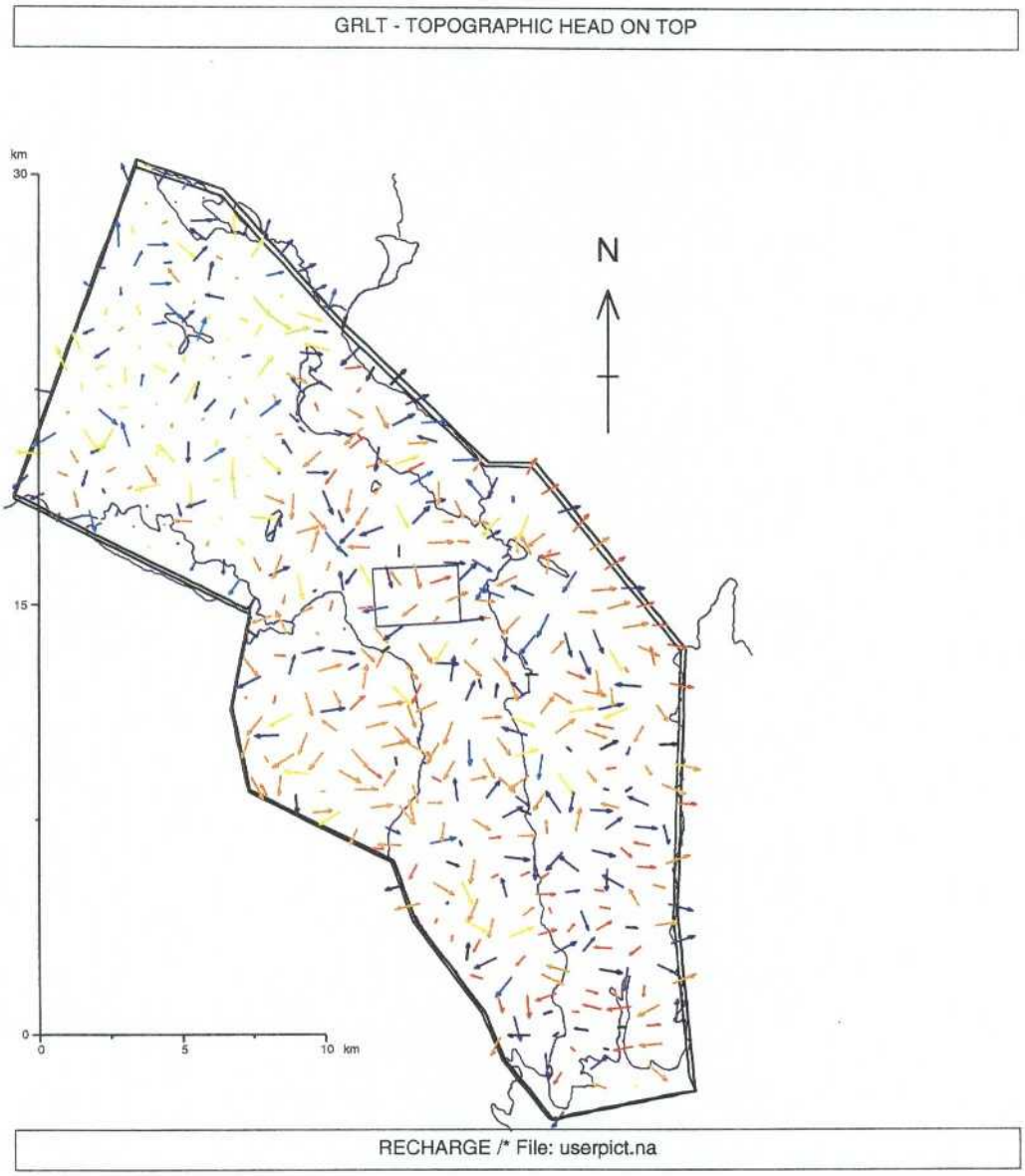

Figure 4.7: Recharge and discharge areas indicated by flow vectors coloured according to the magnitude of the vertical flow component. Recharge range from red to green, green:highest magnitude. Discharge range from violet to cyan, violet: highest discharge. (GRLT).

reasonable fit. A lower hydraulic conductivity 10^{-7}ms^{-1} was set on the top part of the mesh, $Z > 0$, for the high region in the northwest.

Alternatively, the same results could have been achieved by reducing infiltration, but this would not have been consistent with the data supplied, and may have under-predicted flows. Table 4.2 shows the development history of the calibration, i4 corresponds to GRLI.

Table 4.2: Summary of calibration cases

Case	Calibration activity	Calibration values	Remarks
i1	guess K in top 3 layers	$K = 10^{-8}$ms^{-1}	max. head too high
i2	increase K in top 3 layers	$K = 10^{-5}$ms^{-1}	max. head more realistic but too low in NW
i3	decrease K in NW	$K = 10^{-6}$ms^{-1}	surface head more realistic head contours vertical (unrealistic) due to boundary conditions on side
i4	hydrostatic pressure above $z = -50m$, decrease K	$K = 10^{-6}$ms^{-1}	head distribution more realistic

Backward paths, Figure 4.8, are in agreement with the base case. Recharge to the site is from northwest and not more than 1-2 km away. Forward paths all go east toward the coast, and downwards.

Pathlines are also unphysical. Since a uniform infiltration has bee specified over the entire top surface, the whole top surface is forced to be a recharge area. Hence, flow is driven downwards by recharge and discharge takes place at the only place possible - the vertical boundaries.

The situation could have been improved by either of the following two modifications:

- Unsaturated flows could have been considered to give better physics where head is below ground surface. This would have raised predicted heads where currently they are too low, but there still are no mechanisms for terrestial discharge in the system.
- Head could have been specified in rivers and lakes, but this is really forcing discharge to only take place where you allow it, i.e. over-determined for a calibration.

To improve the simulation there is need for something more physical, which allows leakage (discharge) where heads tend to be above surface, and recharge where heads tend to be below. This is where the non-linear boundary condition is used.

4.3.3 Non-linear Infiltration Boundary Condition (GRLN)

The non-linear infiltration boundary condition is described in Section 2.3.3. Such a boundary condition can be approximated by prescribing a recharge term which is a function of head. Because the flow through the surface is then a function of the

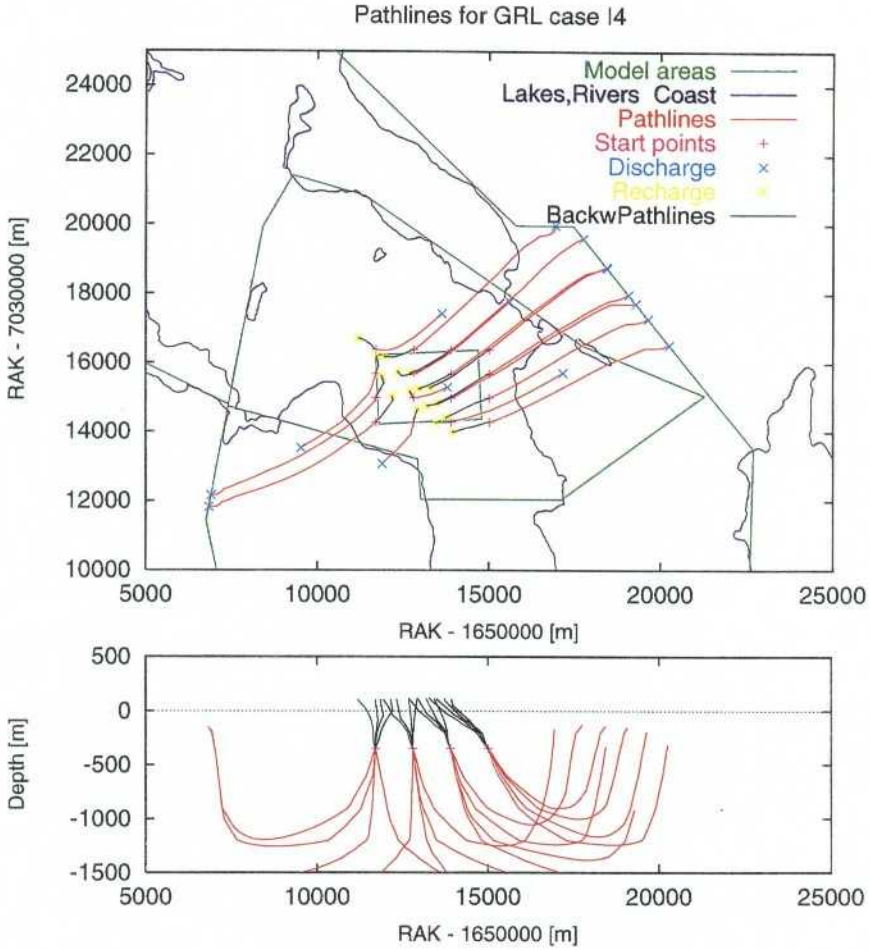

Figure 4.8: Forward and backward pathlines for case GRLI.

dependent variable, the system is non-linear. Nammu uses Newton-Raphson iteration to solve for non-linear problems.

In this model, recharge is bounded by maximum potential infiltration, I, which was set to 50 mm/year. As L goes to zero, see equations in Section 2.3.3,the condition tends to a limiting condition where there is either fixed infiltration, or pressure is fixed at topography, but the non- linearity automates the process of finding which boundary condition is appropriate for any given point. Newton-Raphson iterative methods were employed to solve the non- linearity.

Figure 4.9 shows a plot of total pressure (or $h - z$) at the top surface. This plot shows that the regions of discharge are in good agreement with expectation, i.e. around river valleys, lakes or fracture zones.

Head is clearly affected by conductivity where a smaller conductivity in the top layer would give a closer fit to topography. In order to be able to say more, a number of piezometeric head measurements would be needed.

Both forward and backward pathlines are mostly consistent with the base case (GRLT), Figure 4.10. Note that the backward paths show that there is now more distant recharge from Pratsberget to the Northern part of the site.

4.4 Summary

i) Topography model GRLT, suggests that the semi-regional model GRS, will be extensive enough for predicting flows and pathways at the site.

ii) Flow seems to be delimited by ridges and valleys, and also fracture zones, into a number of flow cells. The semi-regional model contains the flow cell in the vicinity of the site.

iii) It would be fruitful to separate the effects of topography and fracture zones on the flow pattern. This could be done by defining variants of the semi-regional model where the fracture zones are assigned the properties of the rock mass.

iv) The non-linear recharge seems to give realistic results, and enables a calibration of permeability.

v) Hydraulic conductivity of top layers is in the range $1 - 5 \cdot 10^{-6} \mathrm{ms}^{-1}$.

vi) Forward paths diverge away from a region of high head in the middle of the site, which runs North-South. To the East, paths go to a fracture zone along Husån, 1 to 2 km to the East. To the west, particles go either to a fracture zone approximately 2 km to the west, or to the southern fracture zone.

vii) Backward pathlines shows recharge to the site is from the central ridge running North-South above the site. The region of recharge is then above or to the North west of the site.

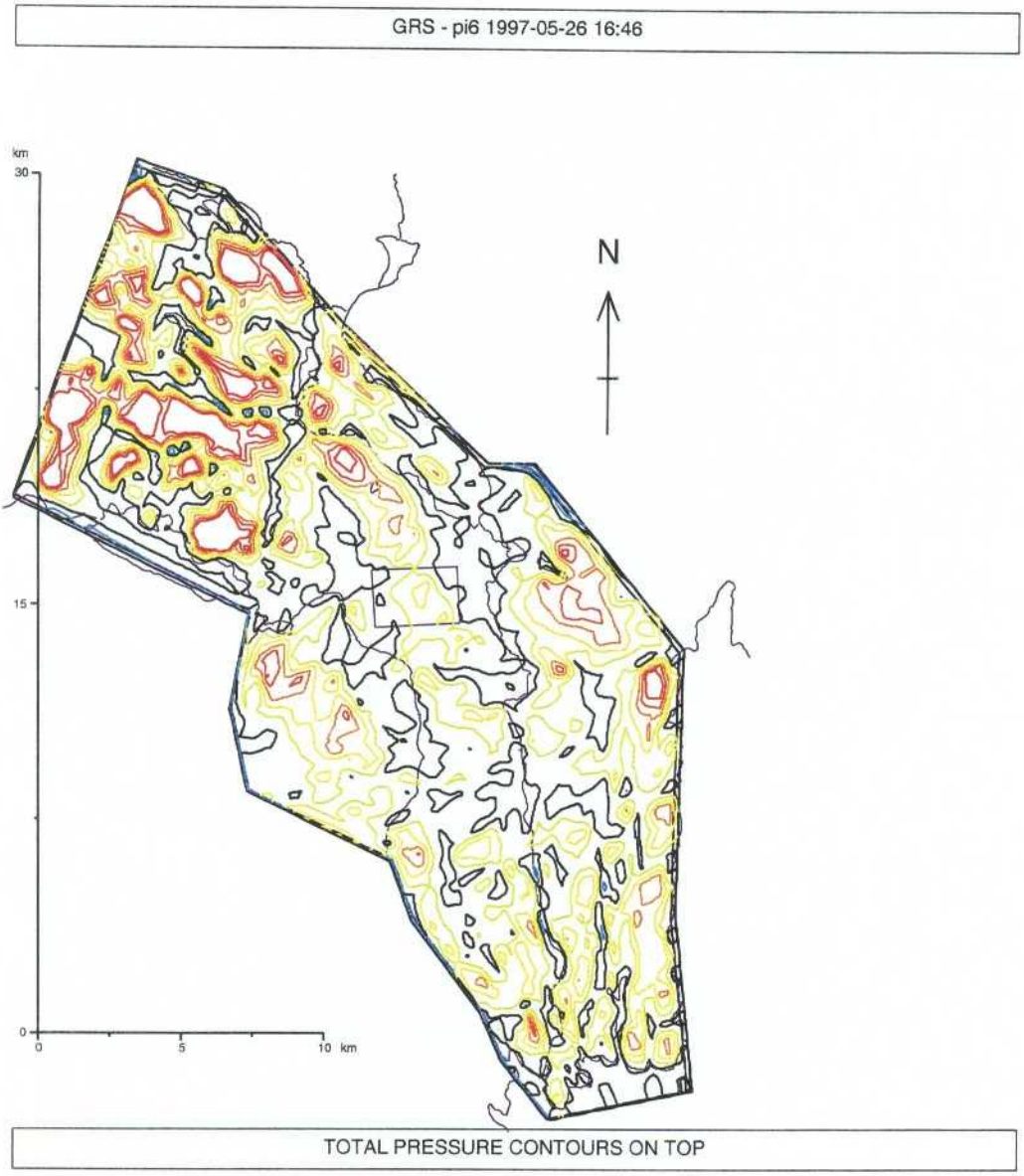

Figure 4.9: Total pressure on top surface. Redish areas show recharge areas and white areas bounded by black contours show discharge. The black contours show the transition from recharge to discharge. Rivers and lakes are outlined in blue. (GRLN)

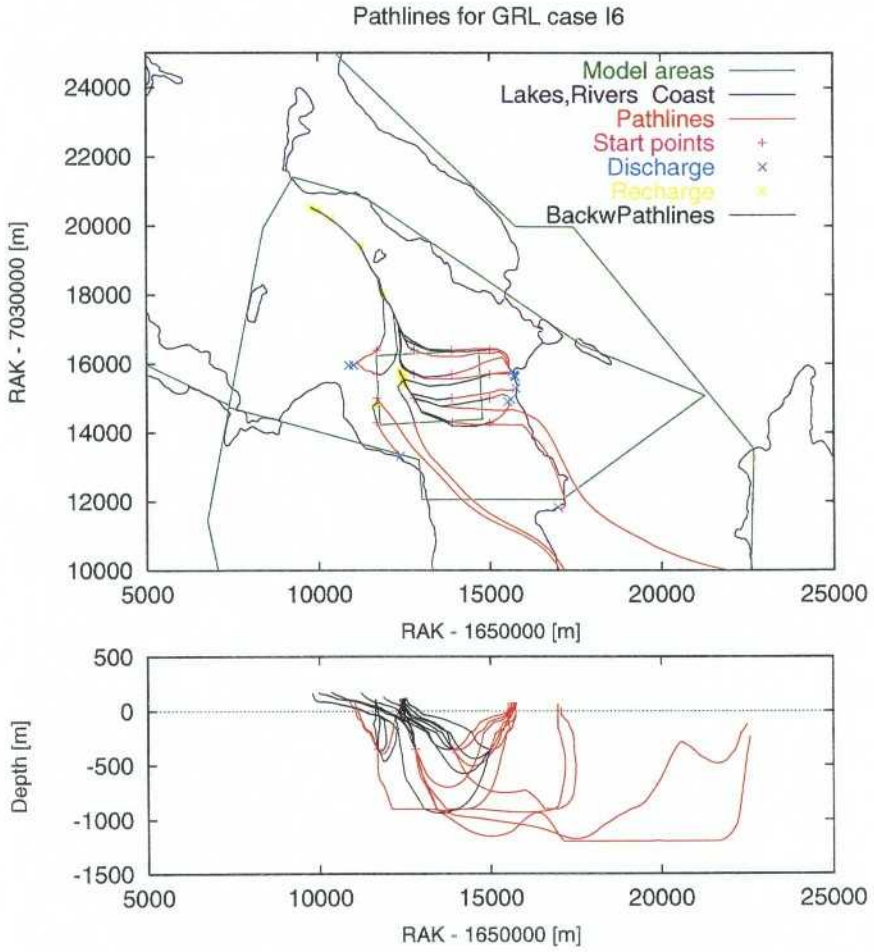

Figure 4.10: Forward and backward pathlines for case (GRLN).

5 Small Regional Model - GRS

5.1 Location and Size

The boundaries of the Small Regional Model (GRS) were chosen using an assumption regarding significant topographic and structural information. The model is about 8 km East-West and 6 km North-South. The area is bounded by fracture zones to the North, West and South. Two parts of the boundary in the east have been located approximately perpendicular to the expected regional flow field i.e. a contour. See Figure 2.1.

Topography data suggests that a general flow pattern within the domain is from the northwest towards the southeast. The high heads in north-west are at approximately 170 m, and the low heads in the East approximately at 30 m.

Several lakes, rivers and streams are included in the model. Gissjön and Gideälven form part of the SouthWest boundary, Hattsjöån and Husån form part of the northern boundary. Gideälven, Husån and Flisbacken flow through the modelled region. Each of these lakes and water courses provide potential areas for groundwater discharge, suggesting there may be substantial terrestial discharge within this model.

5.2 Hydrogeological Properties

The hydrogeological properties used for the small-regional model are the same as was used for the large regional model. Since the properties are poorly understood, in particular the fracture zones, scoping calculations were carried out to quantify parameter sensitivities. See section 5.5.

5.3 Finite-Element Mesh

The finite element grid constructed for the GRS model has the keyvalues outlined in Table 5.1.

Figure 5.1 shows a top view of the mesh. The local site area is outlined as a square in the middle of the model.

The top surface of the model was adjusted to fit the topography of the area. Topography data was obtained using the SKB GIS database.

Table 5.1: Keyvalues for the GRS finite element grid.

Item	Value
Number of elements	38870
Number of nodes	43428
Depth	-1500 masl
Areal extent	10x5 km
Front width	1050
Approximate horizontal resolution	100 m

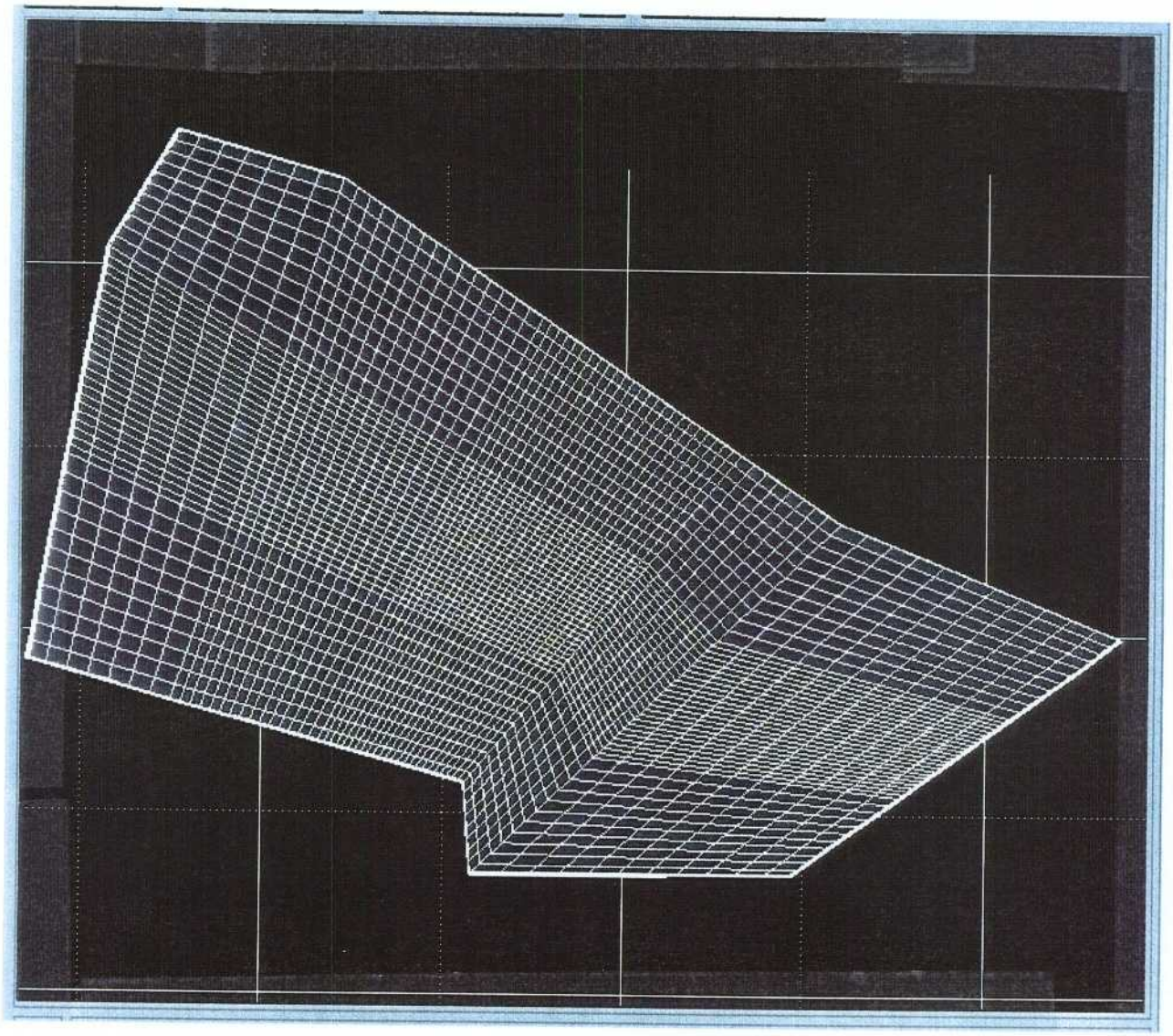

Figure 5.1: Top view of small regional model GRS.

5.4 Boundary Condition Variations

The same type of boundary condition variations have been performed for the small-regional model as was performed for the large regional model with the following exceptions:

- The constant infiltration case has not been simulated.
- In addition a case where the pressures calculated with the large model have been transferred to the boundaries of the semi-regional model.

5.4.1 Specified Pressure (GRST)

The results from this case show the same behaviour as did the specified pressure case using the large model. Hence, the results are consistent with GRLT, compare Figures 4.4 and 5.2.

This means that the local flow cell for the site is no bigger than the size of the small-regional model.

5.4.2 Non-linear Infiltration Boundary Condition (GRSN)

The conclusions draw from this case are consistent with the GRLN case. See Figures 5.5, 5.3 and 5.4.

Again perhaps the conductivity should be smaller to get higher heads. Flux is distributed slightly differently, but there is no significant difference.

5.4.3 Pressures Interpolated from GRLT (GRSL)

In this variation the pressure was interpolated on the top and lateral boundaries using pressure values from the large regional model, GRLT. The reason for interpolating pressure on the top surface is to ensure continuity of pressure along the edges of the model. The pressure on the top surface of the GRLT model was obtained in exactly the same way as for the GRST model, except the grid resolution of the GRLT model is obviously much less. Hence, the boundary conditions on the top surface of GRSL case is very similar to that for GRST only slightly less detailed.

As might be expected, this had no real effect on the flow pattern in the area, see Figure 5.6.

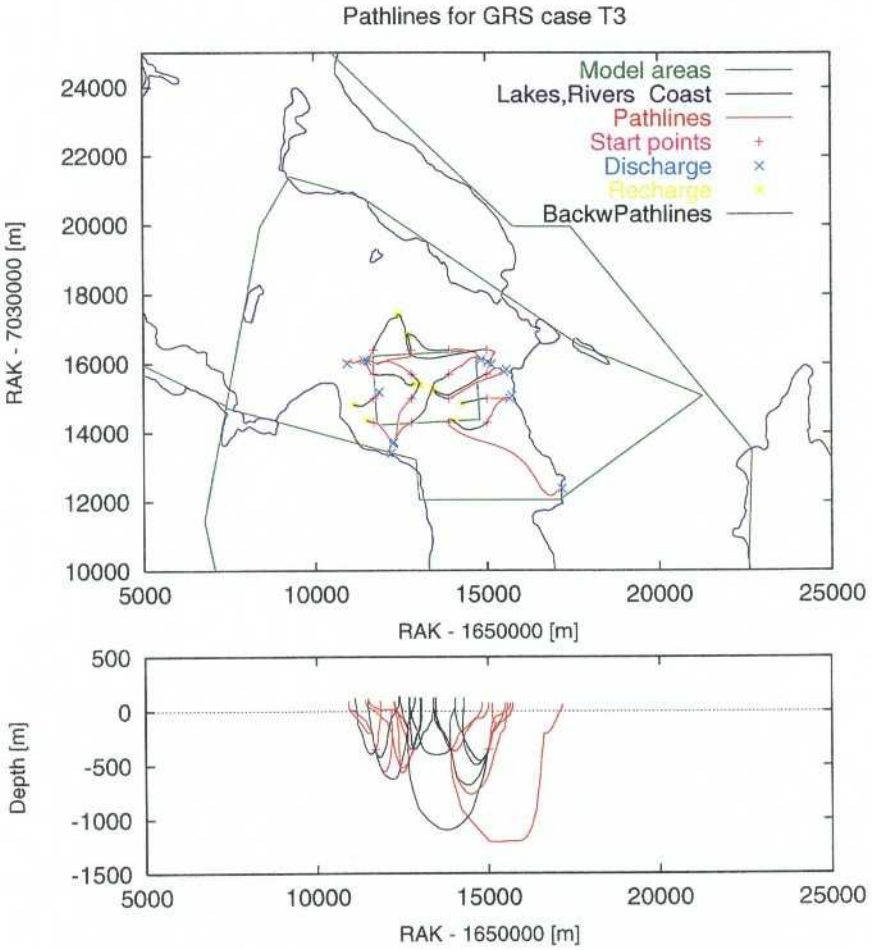

Figure 5.2: Forward and backward pathlines for case GRST.

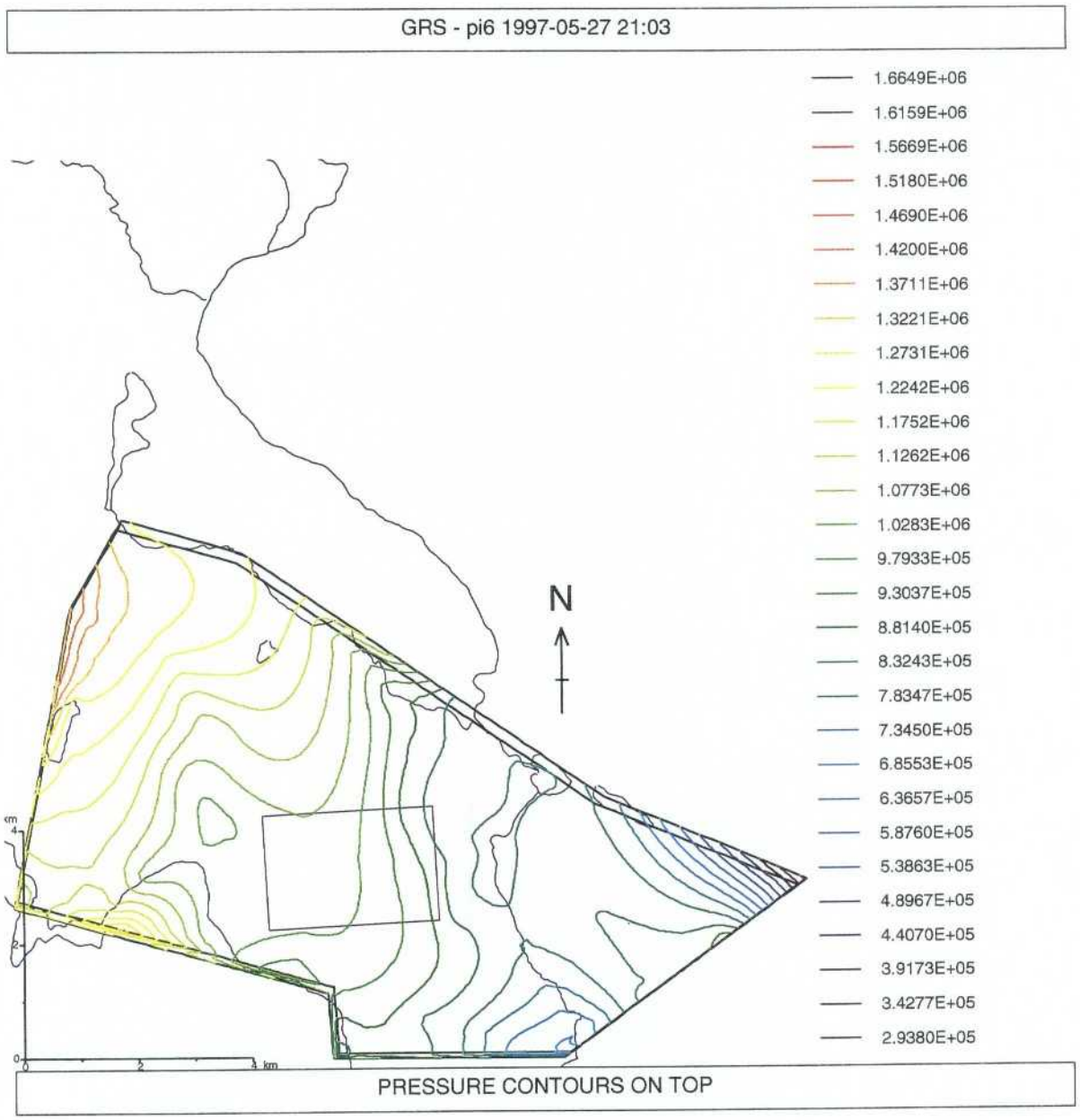

Figure 5.3: Dynamic pressure contours (Pa) on top surface of small regional model with nonlinear recharge (GRSN).

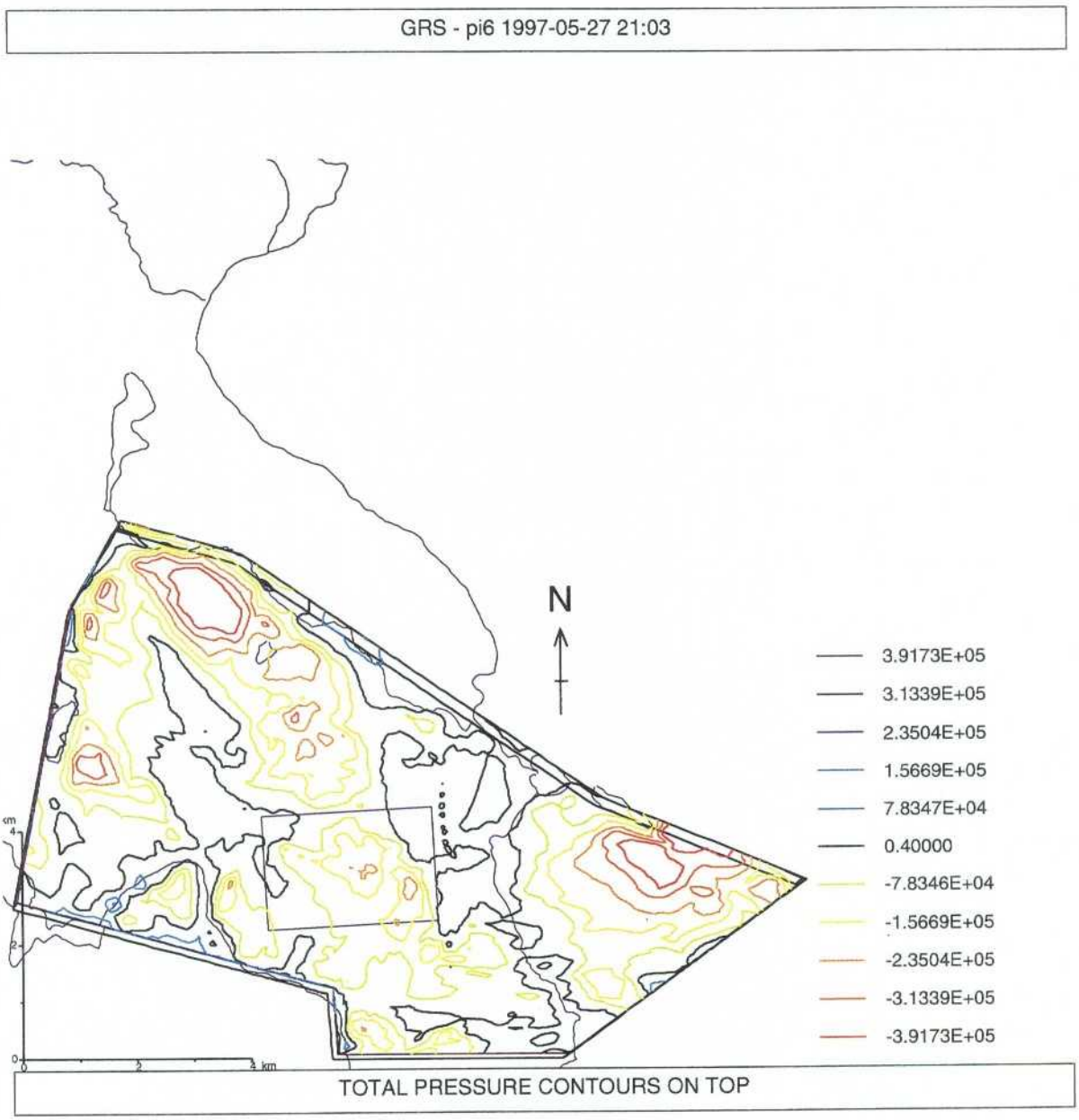

Figure 5.4: Total pressure (Pa) at top surface. Redish areas show recharge areas and white areas bounded by black contours show discharge. The black contours show the transition from recharge to discharge. Rivers and lakes are outlined in blue. (GRSN)

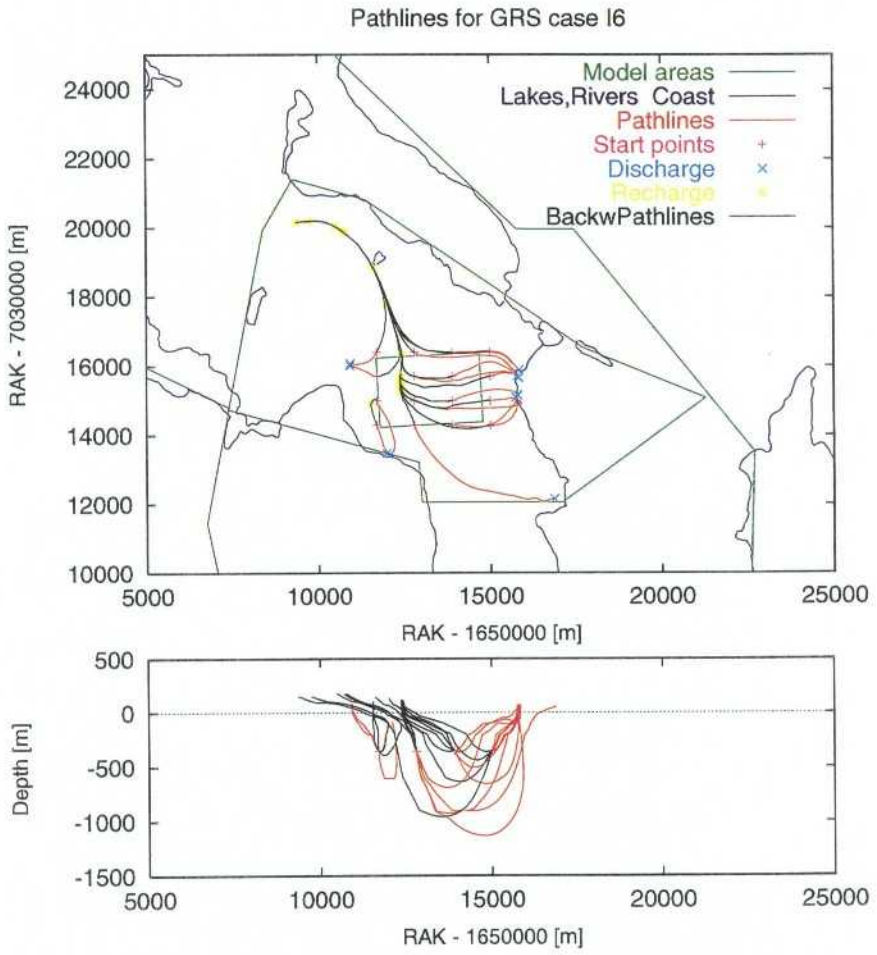

Figure 5.5: Forward and backward pathlines for case GRSN.

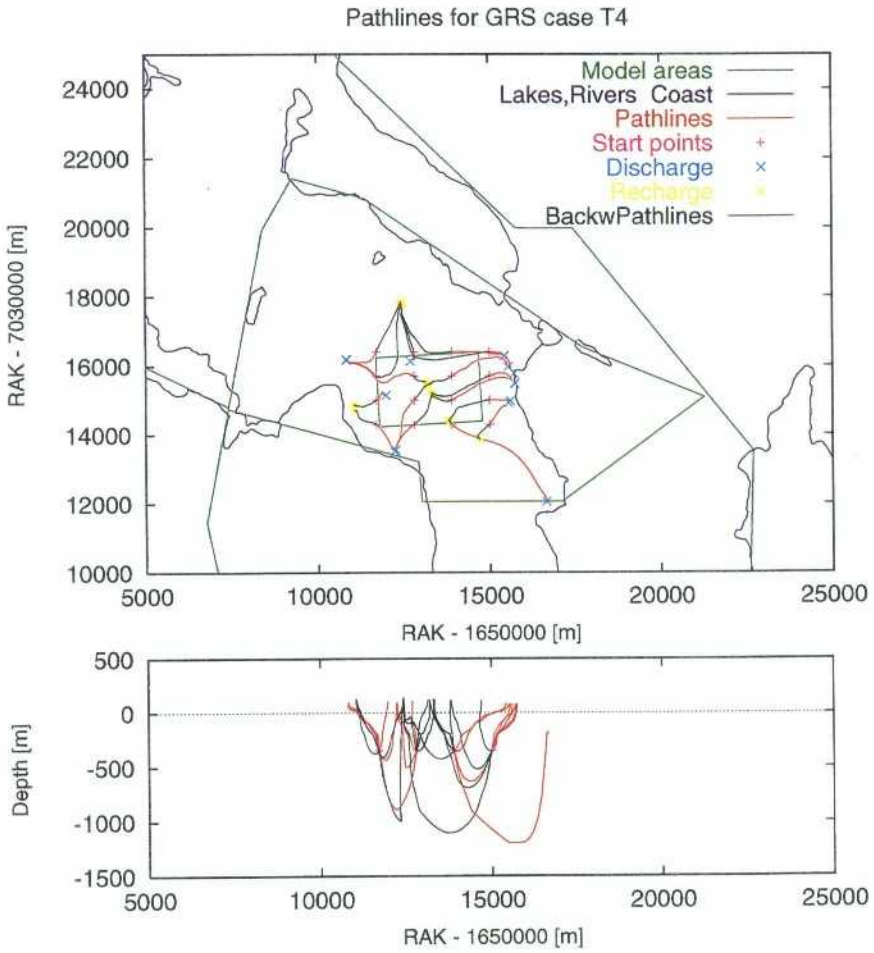

Figure 5.6: Forward and backward pathlines for case GRSL.

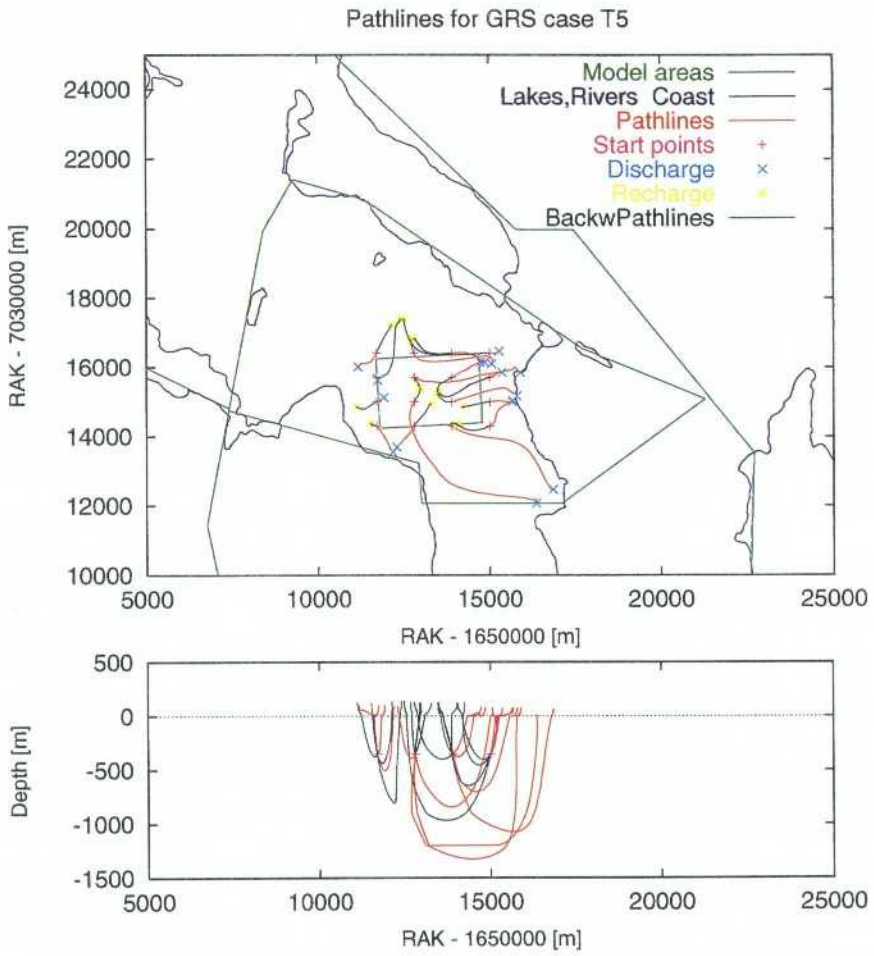

Figure 5.7: Forward and backward pathlines for case GRSU.

5.5 Sensitivity Study

The following set of variations have been included to show the effect of the uncertainties in the hydraulic conductivities and their effect on the general flow pattern.

5.5.1 Uniform Rock Mass Permeability with Depth (GRSU)

In this variation the conductivity of the rock mass was not adjusted to the depth dependence outlined by Walker. Instead the values assigned was $10^{-4.83} ms^{-1}$ in top 3 layers, and $10^{-9.83} ms^{-1}$ in base. The fracture zones have been modelled in the same way as was done in the base case, GRST.

Figure 5.7 show that flow is now deper than in the base case, see Figure 5.2. Discharge/recharge areas are still qualitatively the same as in the base case.

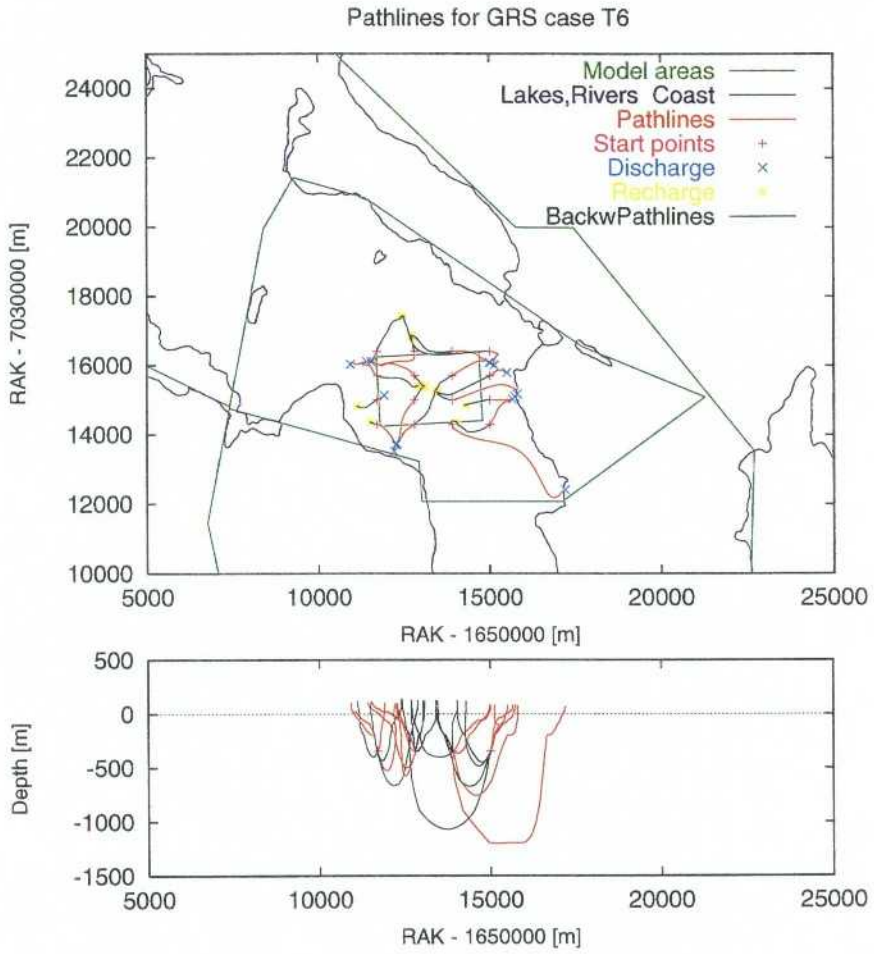

Figure 5.8: Forward and backward pathlines for case GRSFL.

5.5.2 Low Permeability Fracture Zones (GRSFL)

The fracture zones were not included in this variation. Since the contrast between the rock mass and the fracture zones is very low, no significant effect on groundwater flow was seen, see Figure 5.8.

5.5.3 High Permeability Fracture Zones (GRSFH)

In this variation the fracture zone conductivity was increased by two orders of magnitude. Here one can see the effect of increased conductivity in fracture zones on flow arrows. However, the discharge areas are not significantly changed probably due to the small number of fractures around the site area, see Figure 5.9.

5.5.4 Conductivity Anisotropy in the Rock Mass (GRSA)

As stated in Walker et al [*1997*], there are some indications that there may be a regional anisotropy in the conductivity parallel to the direction of the maximum horizontal stress. To investigate the effect of this, a case involving anisotropy has been studied.

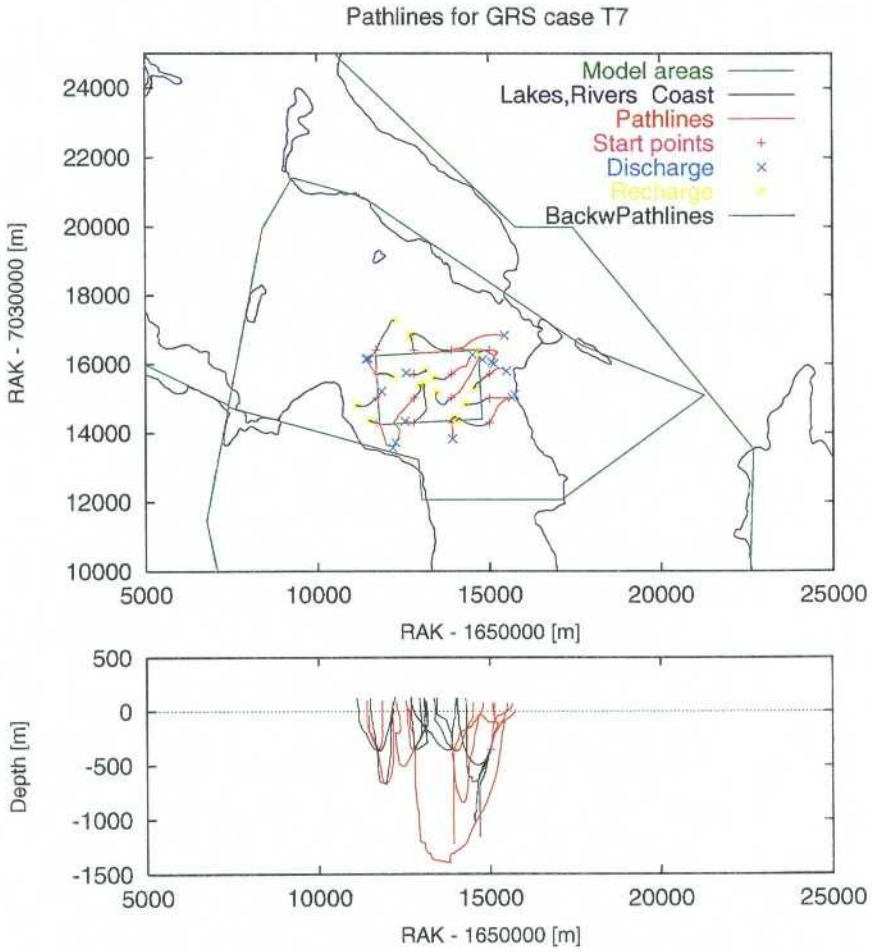

Figure 5.9: Forward and backward pathlines for case GRSFH.

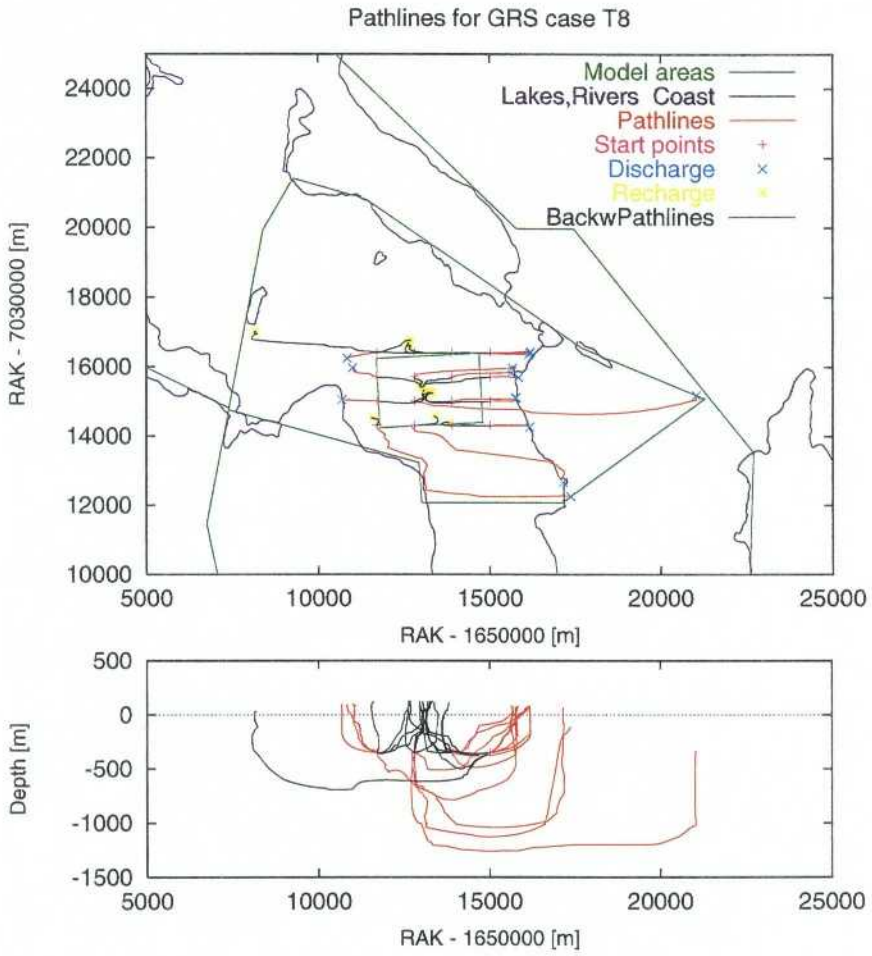

Figure 5.10: Forward and backward pathlines for the anisotropic case. (GRSA)

The anisotropy applied is described in Section 3.3.

As may be seen from Figure 5.10, the applied anisotropy influences the flow pattern by driving the flow more in an east-west direction. Recharge areas are moved southward and discharge locations have moved slightly north.

However, the general discharge areas are roughly the same. The main discharge is to the rivers and lake systems to the northeast of the site.

5.6 Summary

This section summarises the results obtained with the small-regional model, GRS.

i) The boundary condition variations confirm the conclusions drawn with the large regional model GRL, see Section 4.4.

ii) The hydraulic conductivity variations show that even without any fracture zones in the model, GRSFL, no very large scale regional flow patterns influences the

groundwater movement in the hypothetical repository area. The case with increased fracture conductivity decreased the influence area, as expected.

iii) The case with uniform permeabilty for the rock mass with depth, GRSU, showed a small decrease of local topography influence with deeper groundwater movements. However, at the depths of interest these changes did not affect the discharge and recharge areas to any major extent.

iv) The anisotropic case, GRSA, shows some difference from the other cases. However, the magnitude of the anisotropy is not very well understood and no important decisions should be made upon the results from this variation. To better understand the anisotropy a set of anisotropic variations should be performed. The results do however indicate the same general discharge areas, that is the marshes and rivers east and north east of the site area. The recharge has however shifted very much to the south compared to other cases.

6 Discussion

The following Sections discuss various aspects of the results obtained with the models used within this project.

6.1 Differences at Repository Level

6.1.1 Different Boundary Conditions

By comparing the initial Darcy velocity at the start points used for the particle tracks, one may conclude that the two types of boundary conditions (topographic head and non-linear infiltration) give rather similar results as shown in Figure 6.1.

The two cases show the same type of pattern for the Darcy velocity with a slight offset where the Topographic head case GRLT, gives higher velocities compared to the Non-linear case GRLN. The same is true for the particle travel times, there are slightly larger differences here, but these do not change the conclusion that the two types of boundary conditions gives roughly the same answer. The calibration phase could probably have been carried one step further and given an almost perfect match between the two.

6.1.2 Different Models

When comparing the two different models, GRS and GRL, the obvious conclusion from Figure 6.2 must be that the two independent models give almost exactly the same results. It may be noted that for four start points the travel times are longer for GRL than for GRS. These points are in the south west of the site and correspond to the very long paths seen in Figure 4.10 compared to Figure 5.5. The discrepancy is likely to be a result of the coarse discretisation of topography used in the GRLN case giving rise to slightly different distribution of recharge and discharge compared to the GRSN case.

6.2 Location of a Site Scale Model

The results from the present study indicate that a site scale model may be located within the area bounded by the small regional model. It is suggested that if the

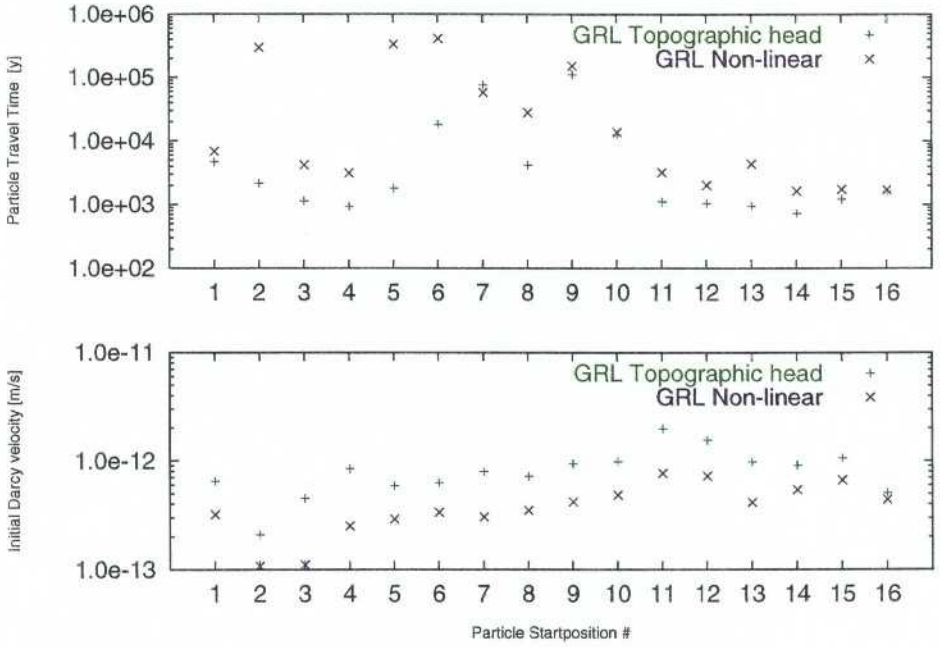

Figure 6.1: Darcy velocity (lower) at particle track startpoints and traveltime (upper) for the particle tracks for the cases GRLT and GRLN.

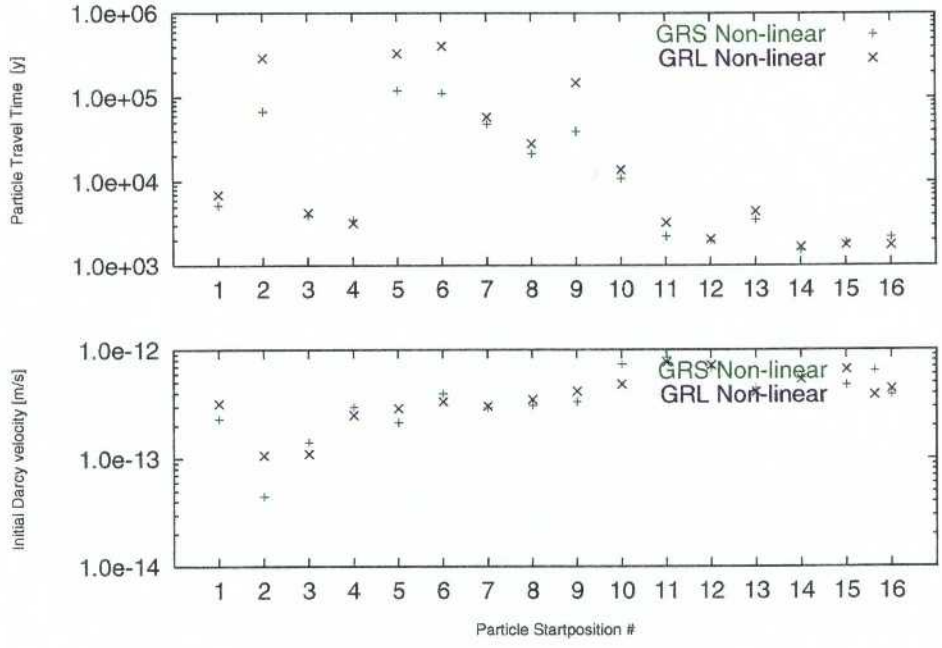

Figure 6.2: Darcy velocity (lower) at particle track startpoints and traveltime (upper) for the particle tracks for the cases GRSN and GRLN.

Hydrastar code is to be used, the model should be oriented in a way indicated by the figure below. This will ensure that all relevant discharge points will be included in the model, by locating the model in this way will minimize the possible errors introduced when applying boundary condition in form of pressures from the GRS model. This is because the site scale model is oriented in the main direction of flow.

The local scale modelling will be carried out using the finite difference code Hydrastar. This only supports simple rectangular geometries, and so it can be difficult to locate a self-contained model which contains all the relevant recharge and discharge areas when the regional flow field is complex. Clearly the results for the local scale model will be sensitive to the boundary conditions supplied by the larger model such as GRS.

However, by making the Hydrastar model sufficiently large with sufficiently large distances from the discharge points this restraint will be minimized.

Since we have a small but noticeable difference in groundwater travel times and Darcy velocities at repository levels between different top surface boundary conditions, see Figure 6.1, one has to make a decision on which of the models to use when generating boundary conditions for the site scale model. The topographic head case is the more conservative of the two whereas the non-linear boundary condition gives a more realistic description of the surface hydrogeology.

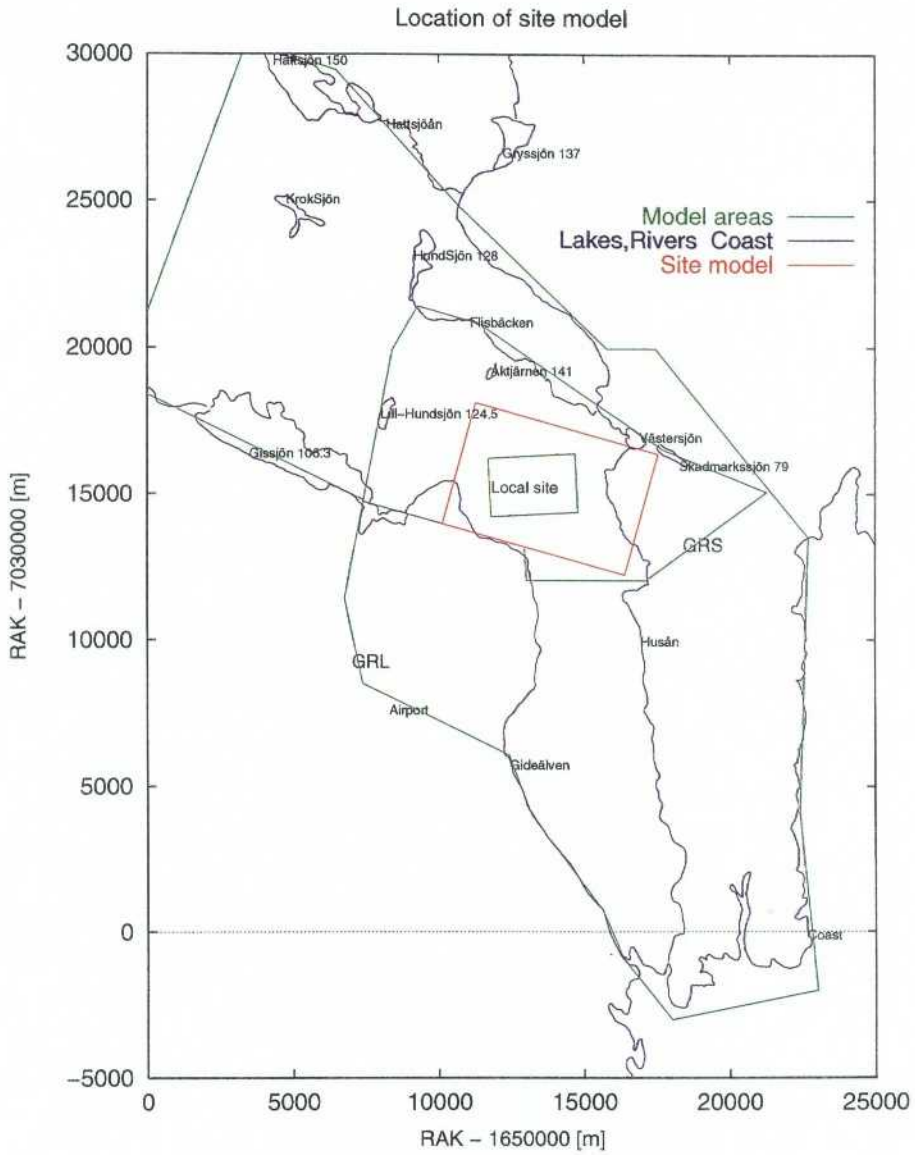

Figure 6.3: Possible location of a site scale Hydrastar model within the smaller regional model, GRS. The areal extent of such a model would be in the order of 5 by 5 km.

7 Conclusions

The present study has addressed the main objectives, which are:

Large-scale groundwater flow patterns: No large-scale regional groundwater flow patterns have been found on depths that are of interest for the present study. In vertical cuts along the preferred direction of flow, which is from the northwest towards the coast in the southeast, one may see larger regional flowpaths at great depths. For instance the Figure 4.5 shows such a cut for the large regional model base case (GRLT). However, the depths at which these paths occur are approximately at a depth below 500 m and are therefore not influencing the hypothetical repository area. Also, the groundwater movements at these depths are very slow.

Locations of significant recharge and discharge: As may be seen from figures in Chapter 5, major recharge areas from the water flowing through the local site area is concentrated to the rivers in the east, Husån, and to south, Gideälven.

Water flowing through a hypothetical repository only has an influence length of a couple of kilometres. Discharge is located at the rivers closest to the site and recharge is drawn from the surrounding hilly areas in the north.

The variations with the small scale regional model were the fracture zones were given a hydraulic conductivity much larger than and equal to the rock mass, show that the major force for the groundwater flow paths within these models are the topography driven flow. Fracture zones only influence the paths to a minor extent.

Influence of different types of boundary conditions: No significant impact was found on the groundwater flow paths from the site area, when using different types of boundary conditions on the smaller regional model. This leads to the conclusion that the small regional model is large enough to be self-contained.

Spatial extent of the regional model required: The conclusion that the small regional model, GRS, is self-contained, is evident when comparing flow patterns from the site area within the large regional model (GRL) with those obtained with the small regional model (GRS).

When designing a regional groundwater flow model, a model that represents the "real" flow domain can be constructed by making fair judgement on probable discharge areas and water divides from local topography and geography information. As shown in this study, this is true even at a site with very low contrast in hydraulic conductivity between the fractured rock and the rock mass. At sites with higher contrast the flow is

probably even more dominated by local features. However, the situation at sites with both a low contrast and a low topographic gradient may be different, but on the other hand this will be reflected by the available topography and geography information

Select the location of a site scale model: If there is a strong wish to incorporate all recharge and discharge areas to and from the site area within the site scale model, the site scale model will be fairly large compared to previous studies.

Supply such a model with appropriate boundary conditions: Since the proposed site scale model is well within the smaller regional model, boundary conditions in the form of groundwater pressures may be transferred from the GRS model to the site scale model. However, as stated in Section 6.1.1, choosing the right model, GRST or GRSN, for supplying the boundary conditions is probably a matter of performing a set of variations with the site model, using the two different boundary condition models.

Sections 4.4 and 5.6 summarises the large regional model GRL and the small regional model GRS respectively.

8 References

Boghammar A., 1992, *Memo: Verifying the Implicit Fracture method, IFZ, using HYDROCOIN Level 1 Case 2,***Kemakta AR 92-19,** Kemakta Konsult AB, 1992.

Carlsson L., Winberg A., Grundfelt B., 1983, *Model calculations of the groundwater flow at Finnsjön, Fjällveden, Gideå and Kamlunge*, **SKBF KBS TR 83-45**, May 1983

Cliffe K.A., Jackson C. P., Morris S. T., 1995, *Assessment Model Validity Document; NAMMU: A program for calculating groundwater flow and transport through porous media.* **SKB AR 95-11**, January 1995

Grundfelt B., Boghammar A., Lindberg H., 1989, *Hypac User's Guide*, **SKB AR 89-22**, 1989

Hermansson J., Hansen L.M., Follin S., 1997, *Update of the geological models of the Gideå study site*, **SKB R-97-05**, March 1997

Rhén I. (ed.), Gustafson G., Stanfors R. and Wikberg P. 1997, *Äspö HRL - Geoscientific evaluation 1997/5. Models based on site characterisation 1986-1995.* , **SKB TR 97-06**, 1997

Timje H., 1983, *Hydrogeological investigations at study site Gideå,* **SKBF AR 83-26**, 1983

Walker D., Rhén I. and Gurban I., 1997, 1997, *Summary of hydrogeologic conditions at Aberg, Beberg and Ceberg.*, **SKB TR 97-zz**, 1997

A Implementation of the implicit fracture zone method

The implicit Fracture Zone method (IFZ) was developed in order to facilitate the generation of fracture zones in a finite element mesh. The hydraulic conductivites of the fracture and the rock mass are averaged over the elements. The method used is based on the fact that the flow through a rectangular box with a fracture zone orthogonally crossing the box, easily can be computed analytically when some assumptions are made.
Figure A.1 shows the general rectangular element with a orthogonally crossing fracture. The following assumptions are made :

1) The fracture zone is of constant width throughout the box.

2) The hydraulic head takes constant values on each face of the box and on the surfaces of the fracture zone.

3) Both the rock-matrix and the fracture zone have constant conductivity and are isotropic media.

The local coordinate system used is parallel to the principal directions of the fracture zone (and rock-matrix). The direction of z is oriented in the normal direction of the fracture zone plane.
The flow through the box in the z-direction is computed through the Darcy law.

$$Q_z = K_z \cdot l_x \cdot l_y \cdot \frac{\Phi_{z1}-\Phi_{z4}}{l_z} = K_m \cdot l_x \cdot l_y \cdot \frac{\Phi_{z1}-\Phi_{z2}}{z2-z1} = \quad \textbf{(13a)}$$

$$= K_f \cdot l_x \cdot l_y \cdot \frac{\Phi_{z2}-\Phi_{z3}}{z3-z2} = K_m \cdot l_x \cdot l_y \cdot \frac{\Phi_{z3}-\Phi_{z4}}{z4-z3} = \quad \textbf{(13b)}$$

where

Qz = flow in the z-direction,

Kz = conductivity in the z-direction,

Km = conductivity for the rock-matrix,

Kf = conductivity for the fracture zone,

Fz = hydraulic head at the point z.

This leads to equations **(14)** **(15)** **(16)** :

$$\Phi_{z1} - \Phi_{z2} = \frac{Q_z \cdot (z2 - z1)}{K_m \cdot l_x \cdot l_y}$$

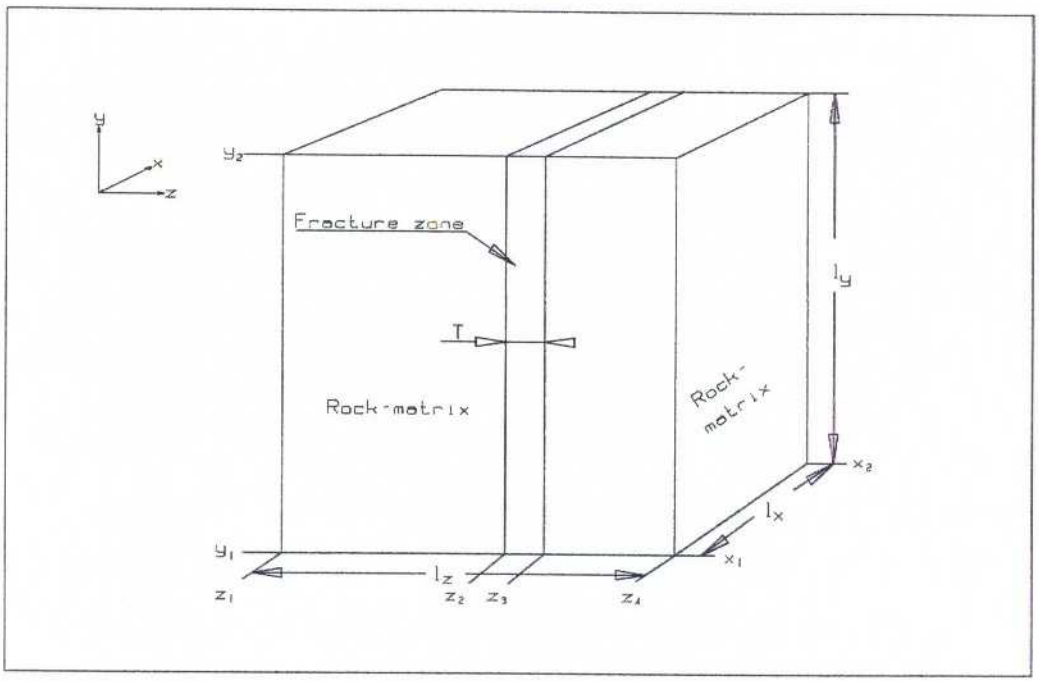

Figure A.1: Definition of rectangular box for implicit fracture zone assignments.

$$\Phi_{z2} - \Phi_{z3} = \frac{Q_z \cdot (z3 - z2)}{K_f \cdot l_x \cdot l_y}$$

$$\Phi_{z3} - \Phi_{z4} = \frac{Q_z \cdot (z4 - z3)}{K_m \cdot l_x \cdot l_y}$$

Adding the equations (14) - (16) :

$$\Phi_{z1} - \Phi_{z4} = \frac{Q_z \cdot ((z2-z1) \cdot (z4-z3))}{K_m \cdot l_x \cdot l_y} + \frac{Q_z \cdot (z3-z2)}{K_f \cdot l_x \cdot l_y} = \frac{Q_z \cdot l_z}{K_z \cdot l_x \cdot l_y} \qquad \textbf{(17)}$$

The last step in equation (17) was derived from the first step in equation (13). Solving for Kz :

$$K_z = l_z \cdot \left[\frac{1}{\frac{(l_z - T)}{K_m} + \frac{T}{K_f}} \right] \qquad \textbf{(18)}$$

The conductivities in the x- and y-directions may be derived in the same way arriving at :

$$K_x = \frac{(l_z - T) \cdot K_m + T \cdot K_f}{l_z} \qquad \textbf{(19)}$$

$$K_y = \frac{(l_z - T) \cdot K_m + T \cdot K_f}{l_z} \qquad \textbf{(20)}$$

As noted Kx, Ky and Kz all depend on Kf, Km, lz and T, but not on lx or ly. In the direction of the fracture zone a mean conductivity is computed as a weighted arithmetic mean, and in the direction normal to the fracture zone plane a weighted harmonic mean is used.

In ground-water flow calculations when finite elements are used, the elements are usually not shaped as boxes and the fracture zones cross the computational domain arbitrarily. The averaging technique described above can still be used in an approximate manner. The following procedure is used for each fracture.

1) Discard those elements that lies outside the fracture plane. Calculation only uses the fracture plane equation, fracture width, element centroid, element max and min values to perform a coarse sort of the elements.

2) If the fracture is bounded : The centroids of the remaining elements are checked to lie within the fracture contour.

3) For all the remaining elements :

- Calculate an approximation of the fracture volume, Fv is calculated by counting the number of 1000 equally spaced points (in the default case 10x10x10) that lie within the fracture. If the fracture is small compared to the element, the number of points are increased so that at least one point may fall within the fracture if the fracture is crossing the element.

- Calculate an approximation of the volume of the element Ev.

- The volume fraction part is defined as Vfp = Fv/Ev

- In the formulas for Kx, Ky and Kz, the values lz and T are used. Since the element is of arbitrary shape, two such values must be computed. The spatial discretization in the physical (sub) horizontal plane are assumed to be of the same magnitude, and this is true in most cases. Further, the fracture zones are set to be either horizontal or vertical (just for the mean calculations). If the fracture zone is horizontal, lz is set equal to the spatial difference in the vertical direction for the element, and if the fracture zone is vertical, lz is set to the spatial difference in one of the other directions. Since nothing is known about the way the fracture zone cuts the element (just the volume is approximated), the fracture zone width used in the mean calculations is set to Tn = Vfp.lz. In such a procedure the most important information is retained.

- Kx, Ky and Kz are computed with the formulas derived above (note that x,y and z correspond to the principal directions of the fracture zone).

- rotate the conductivity tensor (21) into the physical coordinate system, and the tensor will now become full unless the principal directions of the fracture zone coincide with the principal directions of the physical system.

$$\begin{bmatrix} K_x & 0 & 0 \\ 0 & K_y & 0 \\ 0 & 0 & K_z \end{bmatrix} \tag{21}$$

A problem will arise when two or more fractures are crossing the same element. The average procedure will be much more complicated in such a case. This is simplified by calculating the average as if the fracture zone with the highest conductivity of the crossing fracture zones is the only crossing fracture.

The method described can sometimes introduce numerical error compared with traditional finite element generation, However, by increasing the spatial discretization, i.e. increasing the number of elements, the errors will be limited. One may also combine the traditional way of modelling fractured rock with the IFZ-method. Major fracture zones may be modelled explicitly and others using the IFZ-method.
The IFZ method has been described and tested by Boghammar [*1992*].

B Quality Assurance

This appendix records the file locations and edit records for the main NAMMU input data files.

B.1 File Locations

All files are stored on SKB's UNIX workstation sultan (192.36.18.209). The NAMMU input files (.nam) for the GRL model are located in
/export/nammu/2119sr97/ceberg/grl/nam The NAMMU input files (.nam) for the GRS model are located in
/export/nammu/2119sr97/ceberg/grs/nam The NAMMU output files (.out) for the GRL model are located in
/export/nammu/2119sr97/ceberg/grl/nam/out The NAMMU output files (.out) for the GRS model are located in
/export/nammu/2119sr97/ceberg/grs/nam/out The NAMMU postscript files (.ps) for the GRL model are located in
/export/nammu/2119sr97/ceberg/grl/nam/out The NAMMU postscript files (.ps) for the GRS model are located in
/export/nammu/2119sr97/ceberg/grs/nam/out The HYPAC files (.IFG, .IFP, .NLS) for the GRL model are located in
/export/nammu/2119sr97/ceberg/grl/pre The HYPAC files (.IFG, .IFP, .NLS) for the GRS model are located in
/export/nammu/2119sr97/ceberg/grs/pre

B.2 NAMMU Input Files

Table B.1 gives the NAMMU input data files for each of the main cases. The name of the NAMMU input files for post-processing the results to produce postscript graphical files is included. Note: the .out files for each run contain a complete edit history of the HYPAC files used in generating the mesh.

Table B.1: Input files for main cases

Case	NAMMU file	Last edit	HYPAC files	post-processing
GRLT	gridt6	09/04/97	.IFG, .IFP, .NLS,	postt6.nam
GRLI	gridi4	09/04/97	.IFG, .IFP, .NLS,	posti4.nam
GRLN	gridi6	25/06/97	.IFG, .IFP, .NLS,	posti6.nam
GRST	loclt3	10/04/97	.IFG, .IFP, .NLS,	postt3.nam
GRSN	locli6	10/04/97	.IFG, .IFP, .NLS,	posti6.nam
GRSL	locli4	10/04/97	.IFG, .IFP, .NLS,	posti4.nam
GRSFH	loclt7	18/04/97	.IFG, .IFP, .NLS,	postt7.nam
GRSFL	loclt6	10/04/97	.IFG, .IFP, .NLS,	postt6.nam
GRSU	loclt5	11/02/97	.IFG, .IFP, .NLS,	postt5.nam
GRSA	loclt8	26/05/97	.IFG, .IFP, .NLS,	postt8.nam

List of SKB reports

Annual Reports

1977-78
TR 121
KBS Technical Reports 1 – 120
Summaries
Stockholm, May 1979

1979
TR 79-28
The KBS Annual Report 1979
KBS Technical Reports 79-01 – 79-27
Summaries
Stockholm, March 1980

1980
TR 80-26
The KBS Annual Report 1980
KBS Technical Reports 80-01 – 80-25
Summaries
Stockholm, March 1981

1981
TR 81-17
The KBS Annual Report 1981
KBS Technical Reports 81-01 – 81-16
Summaries
Stockholm, April 1982

1982
TR 82-28
The KBS Annual Report 1982
KBS Technical Reports 82-01 – 82-27
Summaries
Stockholm, July 1983

1983
TR 83-77
The KBS Annual Report 1983
KBS Technical Reports 83-01 – 83-76
Summaries
Stockholm, June 1984

1984
TR 85-01
Annual Research and Development Report 1984
Including Summaries of Technical Reports Issued during 1984. (Technical Reports 84-01 – 84-19)
Stockholm, June 1985

1985
TR 85-20
Annual Research and Development Report 1985
Including Summaries of Technical Reports Issued during 1985. (Technical Reports 85-01 – 85-19)
Stockholm, May 1986

1986
TR 86-31
SKB Annual Report 1986
Including Summaries of Technical Reports Issued during 1986
Stockholm, May 1987

1987
TR 87-33
SKB Annual Report 1987
Including Summaries of Technical Reports Issued during 1987
Stockholm, May 1988

1988
TR 88-32
SKB Annual Report 1988
Including Summaries of Technical Reports Issued during 1988
Stockholm, May 1989

1989
TR 89-40
SKB Annual Report 1989
Including Summaries of Technical Reports Issued during 1989
Stockholm, May 1990

1990
TR 90-46
SKB Annual Report 1990
Including Summaries of Technical Reports Issued during 1990
Stockholm, May 1991

1991
TR 91-64
SKB Annual Report 1991
Including Summaries of Technical Reports Issued during 1991
Stockholm, April 1992

1992
TR 92-46
SKB Annual Report 1992
Including Summaries of Technical Reports Issued during 1992
Stockholm, May 1993

1993
TR 93-34
SKB Annual Report 1993
Including Summaries of Technical Reports Issued during 1993
Stockholm, May 1994

1994

TR 94-33

SKB Annual Report 1994

Including Summaries of Technical Reports Issued during 1994

Stockholm, May 1995

1995

TR 95-37

SKB Annual Report 1995

Including Summaries of Technical Reports Issued during 1995

Stockholm, May 1996

1996

TR 96-25

SKB Annual Report 1996

Including Summaries of Technical Reports Issued during 1996

Stockholm, May 1997

List of SKB Technical Reports 1997

TR 97-01

Retention mechanisms and the flow wetted surface – implications for safety analysis

Mark Elert

Kemakta Konsult AB

February 1997

TR 97-02

Äspö HRL – Geoscientific evaluation 1997/1. Overview of site characterization 1986–1995

Roy Stanfors[1], Mikael Erlström[2], Ingemar Markström[3]

[1] RS Consulting, Lund

[2] SGU, Lund

[3] Sydkraft Konsult, Malmö

March 1997

TR 97-03

Äspö HRL – Geoscientific evaluation 1997/2. Results from pre-investigations and detailed site characterization. Summary report

Ingvar Rhén (ed.)[1], Göran Bäckblom (ed.)[2], Gunnar Gustafson[3], Roy Stanfors[4], Peter Wikberg[2]

[1] VBB Viak, Göteborg

[2] SKB, Stockholm

[3] VBB Viak/CTH, Göteborg

[4] RS Consulting, Lund

May 1997

TR 97-04

Äspö HRL – Geoscientific evaluation 1997/3. Results from pre-investigations and detailed site characterization. Comparison of predictions and observations. Geology and mechanical stability

Roy Stanfors[1], Pär Olsson[2], Håkan Stille[3]

[1] RS Consulting, Lund

[2] Skanska, Stockholm

[3] KTH, Stockholm

May 1997

TR 97-05

Äspö HRL – Geoscientific evaluation 1997/4. Results from pre-investigations and detailed site characterization. Comparison of predictions and observations. Hydrogeology, groundwater chemistry and transport of solutes

Ingvar Rhén[1], Gunnar Gustafson[2], Peter Wikberg[3]

[1] VBB Viak, Göteborg

[2] VBB Viak/CTH, Göteborg

[3] SKB, Stockholm

June 1997

TR 97-06

Äspö HRL – Geoscientific evaluation 1997/5. Models based on site characterization 1986–1995

Ingvar Rhén (ed.)[1], Gunnar Gustafson[2], Roy Stanfors[4], Peter Wikberg[4]

[1] VBB Viak, Göteborg

[2] VBB Viak/CTH, Göteborg

[3] RS Consulting, Lund

[4] SKB, Stockholm

October 1997

TR 97-07

A methodology to estimate earthquake effects on fractures intersecting canister holes

Paul La Pointe, Peter Wallmann, Andrew Thomas, Sven Follin

Golder Associates Inc.

March 1997

TR 97-08

Äspö Hard Rock Laboratory Annual Report 1996

SKB

April 1997

TR 97-09

A regional analysis of groundwater flow and salinity distribution in the Äspö area

Urban Svensson

Computer-aided Fluid Engineering AB

May 1997

TR 97-10
On the flow of groundwater in closed tunnels. Generic hydrogeological modelling of nuclear waste repository, SFL 3–5
Johan G Holmén
Uppsala University/Golder Associates AB
June 1997

TR 97-11
Analysis of radioactive corrosion test specimens by means of ICP-MS. Comparison with earlier methods
R S Forsyth
Forsyth Consulting
July 1997

TR 97-12
Diffusion and sorption properties of radionuclides in compacted bentonite
Ji-Wei Yu, Ivars Neretnieks
Dept. of Chemical Engineering and Technology, Chemical Engineering, Royal Institute of Technology, Stockholm, Sweden
July 1997

TR 97-13
Spent nuclear fuel – how dangerous is it? A report from the project "Description of risk"
Allan Hedin
Swedish Nuclear Fuel and Waste Management Co,
Stockholm, Sweden
March 1997

TR 97-14
Water exchange estimates derived from forcing for the hydraulically coupled basins surrounding Äspö island and adjacent coastal water
Anders Engqvist
A & I Engqvist Konsult HB, Vaxholm, Sweden
August 1997

TR 97-15
Dissolution studies of synthetic soddyite and uranophane
Ignasi Casas[1], Isabel Pérez[1], Elena Torrero[1], Jordi Bruno[2], Esther Cera[2], Lara Duro[2]
[1] Dept. of Chemical Engineering, UPC
[2] QuantiSci SL
September 1997

TR 97-16
Groundwater flow through a natural fracture. Flow experiments and numerical modelling
Erik Larsson
Dept. of Geology, Chalmers University of Technology, Göteborg, Sweden
September 1997

TR 97-17
A site scale analysis of groundwater flow and salinity distribution in the Äspö area
Urban Svensson
Computer-aided Fluid Engineering AB
October 1997

TR 97-18
Release of segregated nuclides from spent fuel
L H Johnson, J C Tait
AECL, Whiteshell Laboratories, Pinawa, Manitoba, Canada
October 1997

TR 97-19
Assessment of a spent fuel disposal canister. Assessment studies for a copper canister with cast steel inner component
Alex E Bond, Andrew R Hoch, Gareth D Jones, Aleks J Tomczyk, Richard M Wiggin, William J Worraker
AEA Technology, Harwell, UK
May 1997

TR 97-20
Diffusion data in granite. Recommended values
Yvonne Ohlsson, Ivars Neretnieks
Department of Chemical Engineering and Technology, Chemical Engineering, Royal Institute of Technology, Stockholm, Sweden
October 1997

ISSN 0284-3757
CM Gruppen AB, Bromma, 1996